Structural Insights into the Nature of Fe 0 and Fe I Low-Valent Species Obtained upon the Reduction of Iron Salts by Aryl Grignard Reagents

Martin Clémancey, Thibault Cantat, Geneviève Blondin, Jean-Marc Latour, Pierre Dorlet, Guillaume Lefèvre

Structural insights into the nature of Fe^0 and Fe^I low-valent species obtained upon reduction of Iron salts by Aryl Grignard reagents.

Martin Clémancey,[§] Thibault Cantat,[†] Geneviève Blondin,[§] Jean-Marc Latour,[§] Pierre Dorlet,*[‡] and Guillaume Lefèvre*[†]*

[§] University of Grenoble Alpes, LCBM/PMB and CEA, BIG/CBM/PMB and CNRS, LCBM UMR 5249, PMB, 38000 Grenoble, France

[†] NIMBE, CEA, CNRS, Université Paris-Saclay, Gif-sur-Yvette, France

[‡] Institute for Integrative Biology of the Cell (I2BC), CEA, CNRS, Univ. Paris-Sud, Université Paris-Saclay, Gif-sur-Yvette, France

Abstract

Mechanistic studies of the reduction of Fe^{III} and Fe^{II} salts by aryl Grignard reagents in toluene:THF mixtures in the absence of supporting ligand are reported, as well as structural insights regarding the nature of the low-valent Fe species obtained at the end of this reduction process. It is shown that several reduction pathways can be followed, depending on the starting Fe precursor. We demonstrate moreover that these pathways lead to a mixture of Fe^0 and Fe^I complexes regardless of the nature of the precursor. Mössbauer and ^1H NMR spectroscopies suggest that diamagnetic 16-electron bis-arene complexes such as $(\eta^4\text{-}C_6H_5Me)_2Fe^0$ can be formed as major species (85% of the overall iron quantity). The formation of a η^6-arene-ligated low-spin Fe^I complex as a minor species (accounting for ca. 15% of the overall iron quantity) is attested by Mössbauer spectroscopy, as well as by cw-EPR and pulse-EPR (HYSCORE) spectroscopies. The nature of the Fe^I coordination sphere is discussed by means of isotopic labelling experiments and DFT calculations. It is shown that the most likely low-spin Fe^I candidate obtained in these systems is a bis-phenyl arene-stabilized species $[(\eta^6\text{-}C_6H_5Me)Fe^IPh_2]^-$ exhibiting an idealized C_{2V} topology. This enlightens the nature of the lowest valence states accommodated by iron during the reduction of Fe^{III} and Fe^{II} salts by aryl Grignard reagents in the absence of any additional co-ligand, which remained so far rather unknown. The reactivity of these low-valent Fe^I and Fe^0 complexes in aryl-heteroaryl Kumada cross-coupling conditions has also been investigated, and it is showed that the zerovalent Fe^0 species can be used efficiently as a precursor in this reaction, whereas the Fe^I oxidation state does not exhibit any reactivity.

Keywords

Low-valent iron, EPR spectroscopy, Mössbauer spectroscopy, DFT

Introduction

To reach a broad scope of cross-coupling reactions based on iron catalysis is an appealing alternative to the noble-metal-based cross-coupling catalysis, because iron is a cost-efficient, abundant and non-toxic metal.[1] The first iron-catalyzed cross-coupling reactions were reported by Kochi in the early 1970s and they involved vinylic halides and alkyl Grignard reagents (Scheme 1a).[2a,b] Several decades later, the methodology was successfully extended to heteroaryl halides and aryl Grignard reagents by Fürstner et al. (Scheme 1b) and was further explored by other groups.[2c-n] This coupling reaction was first developed with simple iron catalysts, e.g. Fe(β-diketonate)$_3$, and $FeCl_2$ or $FeCl_3$, without any stabilizing co-ligand. Iron salts combined with N-Heterocyclic Carbenes (NHCs) and with fluoride anions proved to circumvent the homocoupling of the Grignard reagent, which was often observed as a side reaction.[3]

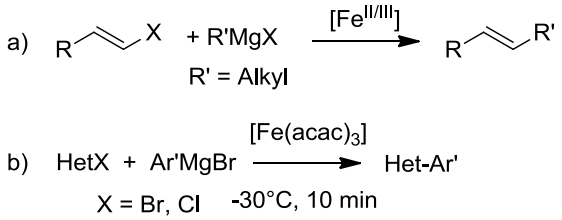

Scheme 1. Representative milestones in Fe-catalyzed C–C cross-couplings.

From a mechanistic standpoint, several low-valent iron species were suggested as catalytically relevant (e.g. Fe^{-II}, Fe^{0}, Fe^{I} and Fe^{II} species).[4] Fürstner reported in 2005 that homoleptic "super-ate Fe^{II}-complexes" such as $[(Me_4Fe^{II})(MeLi)][Li(OEt_2)]_2$ could exhibit activity towards organic electrophiles in catalytic and stoichiometric cross-coupling processes.[5] Later, the group of Bedford demonstrated that (bis-diphosphine)Fe^{I} mono-aryl complexes were catalytically active in Negishi-type couplings.[6] The reactivity of *in-situ*-generated Fe^{I} species with organic halides (e.g. aryl,[7a] benzyl[7b], or alkyl derivatives[7c]) has been extensively investigated ever since, EPR spectroscopy being often used as an experimental characterization tool to support the involvement of d^7-Fe^{I} complexes. Several reports focused on the possibility of promoting C─C bond formation reactions using tmeda-[7d] and NHC-stabilized[7e-g] Fe^{II} well-defined species were also published recently. In 2015, the group of Neidig reported that the catalytic activity observed in aryl-alkyl Kumada and Suzuki-Miyaura cross-couplings catalyzed by SciOPP-stabilized systems was due to (SciOPP)$Fe^{II}(Ph)_n$ species (SciOPP = C_6H_4-1,2-$(P(C_6H_3$-3,5-$tBu_2)_2)_2$; n = 1 and 2). They also demonstrated that the bis-phenylated species (SciOPP)$Fe^{II}(Ph)_2$ was less selective and led to significant amount of β-elimination products when secondary alkyl halides are employed as electrophiles. Importantly, it was also showed that Fe^{I} intermediates were obtained as minor reduced byproducts as well as catalytically non-relevant Fe^{0} species.[8] The authors demonstrated in this report the importance of the spin titration of EPR-detected species, since iron oxidation states with an integer electronic spin (more specifically Fe^{II} and Fe^{0}) cannot be detected by this technique. The matter of the identification of the catalytically active species is also crucial and still unanswered for systems based on the use of coligand-free iron salts and aryl Grignard reagents as reductants, as well as the exact nature of the metal oxidation states reached upon reduction under these conditions. Such coligand-free systems are more difficult to

investigate due to the absence of stabilizing ligands, since the low-valent iron species have consequently shorter lifetimes and tend to lead to aggregates. A very representative case is the recent advancement made in the reduction of iron salts with methyl nucleophiles, with the delineation of the structure of the S = 1/2 species observed by Kochi in his first reports when reducing ferric chloride with the alkyl Grignard MeMgBr in THF[2b]. This structure has remained unknown during almost 40 years, and Neidig recently reported that this species was a cluster involving 8 iron centers ($[Fe_8Me_{12}]^-$), which could exhibit catalytic activity when associated with an excess of MeMgBr.[9] Therefore, the question of both the identification and the titration of half-integer spin iron species which have been detected in similar systems remains crucial. In this paper, we focused our investigations on the delineation of the nature of reduced metallic intermediates obtained upon reaction of simple Fe^{III} or Fe^{II} salts with aryl Grignard reagents (herein PhMgBr or PhMgCl) in the absence of stabilizing co-ligand. Some mechanistic insights regarding the redox events involved in the reduction steps (bielectronic or monoelectronic transfers) have been gained. We demonstrate that the same low-spin Fe^{I} species can be obtained upon reduction of salts such as $Fe(acac)_n$ or $FeCl_n$ (n = 2, 3) by PhMgBr in toluene:THF (10:1) mixtures. As evidenced by radical-trapping experiments, the Fe^{I} species originate from successive monoelectronic reductions of Fe^{II} and Fe^{III} precursors. Disproportionation of transient Fe^{II} intermediates also provides Fe^{I} oxidation state, associated with Fe^{III} species. For the first time, structural insights are gained for this Fe^{I} complex. cw-EPR and pulsed-EPR spectroscopies were used to investigate its coordination sphere, which proved to feature η^6-coordination of the solvent, as well as σ-coordination of anionic $C_6H_5^-$ ligands originating from PhMgX (X = Cl, Br). However, Fe^{I} oxidation state only represents ca. 15 % of the overall iron quantity, the distribution of the metallic species being quickly dominated by the formation of diamagnetic Fe^0

species as evidenced by Mössbauer spectroscopy. The nuclear parameters obtained for this Fe^0 species are moreover similar to already reported complexes featuring bis-arene coordination of the metal. The presence of Fe^0-arene ligation is also confirmed by low-temperature ^1H NMR spectroscopy. Fe^0 molecular species then evolve to the formation of metallic aggregates. These results are supported by DFT calculations, which were performed to investigate the electronic structure of the Fe^I and Fe^0 above-mentioned species. Moreover, it is demonstrated at the end of the manuscript that the zerovalent Fe^0 complex can be used as an efficient precursor in Kumada aryl-heteroaryl cross-couplings, whereas the Fe^I species remains unreactive in the same conditions.

Experimental section

General considerations. All the samples were prepared at 25°C in a recirculating mBraun LabMaster DP inert atmosphere (Ar) drybox and vacuum Schlenk lines. Glassware was dried overnight at 60 ºC before use. NMR spectra were obtained using a Bruker DPX 200 MHz spectrometer. Chemical shifts for ^1H NMR spectra were referenced to solvent impurities (herein THF). Solvents (h_8-toluene, d_8-toluene, d_8-tetrahydrofuran) were dried over a Na/benzophenone mixture, and distilled before used.

EPR spectroscopy. cw-EPR spectra were recorded on a Bruker Elexsys E500 spectrometer equipped with a continuous flow cryostat (Oxford). Pulse EPR experiments were performed on a Bruker Elexsys E580 spectrometer at liquid helium temperatures. 4-pulse hyperfine sublevel correlation (HYSCORE) spectra were recorded with the usual four-pulse sequence $(\pi/2)_y$-τ-$(\pi/2)_y$-t_1-$(\pi)_y$-t_2-$(\pi/2)_y$ with pulse lengths $t_{\pi/2} = t_\pi = 24$ ns and different amplitudes for $\pi/2$ and π pulses. The size of the data was 256x256, the time intervals t_1 and t_2

were varied from 120 ns to 4200 ns in steps of 16 ns. A four-step phase cycle was used to eliminate unwanted echoes. The time domain spectra were baseline corrected and zero-filled before 2D Fourier transformation to yield the frequency maps. Pulse EPR data were processed and simulations were performed by using the Easyspin software package and routines locally written with Matlab (The Mathworks, Inc.).

DFT computation. DFT computations were performed using Gaussian09 version D.01. Unless specified otherwise, all structures were characterized as minima by frequency analysis (no imaginary frequency), and were optimized without geometrical constraint. Unrestricted DFT methods were applied (see SI for the detailed methods).

Mössbauer spectroscopy. Mössbauer spectra were recorded at 5 K on a low-field Mössbauer spectrometer equipped with a Janis CCR 5K cryostat, or at 4.2 or 20 K on a strong-field Mössbauer spectrometer equipped with an Oxford Instruments Spectromag 4000 cryostat containing an 8 T split-pair superconducting magnet. Both spectrometers were operated in a constant acceleration mode in transmission geometry. The isomer shifts are referenced against that of a metallic iron foil at room-temperature. Analysis of the data was performed with the program WMOSS (WMOSS4 Mössbauer Spectral Analysis Software, www.wmosss.org, 2009-2015) and a homemade program[10]. Computational modellings of Mössbauer parameters were carried out using ORCA software (version 3.0.3) at a BP86 – TZVP / CP(PPP) (Fe) level (see SI for the detailed methods).

Synthesis of isotopically enriched products. $^{57}FeCl_2$ was synthesized as follows. Elemental 94%-enriched ^{57}Fe was heated under dry *in-situ*-generated chlorine atmosphere at 350°C during 15 minutes. Dry chlorine was obtained by adding dropwise anhydrous sulfuric acid into a commercial bleach solution; the resulting chlorine gas was then dried by bubbling into

sulfuric acid (98%). $^{13}C_6H_5MgBr$ was synthesized according to a reported microscale method using commercial $^{13}C_6H_5Br$ and elemental magnesium.[11]

Results and discussion

Role of the nature of the precursor in the reduction mechanism. The reduction of $Fe(acac)_3$ by 1 equiv. of PhMgBr in d_8-THF was monitored by ^1H NMR. $Fe(acac)_3$ was fully consumed, whereas $Fe(acac)_2$, acacMgBr and PhPh were characterized by their ^1H NMR signals ($Fe(acac)_2$: -31,5 ppm (12H, CH_3), CH not detected in THF; acacMgBr : 5.2 ppm (1H, CH)), attesting that they were quantitatively obtained within 5 minutes at room temperature, leading to a bright yellow solution (Scheme 2a).[12]

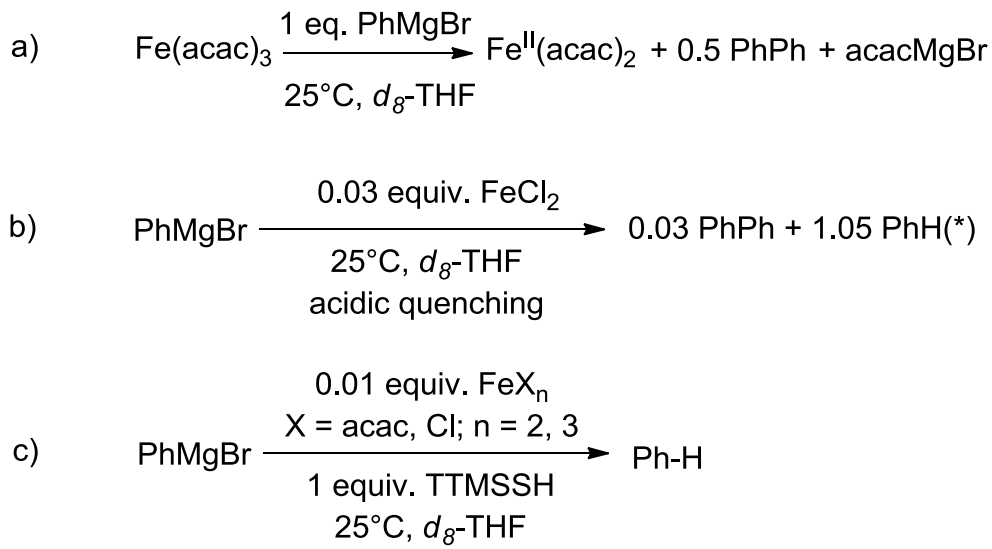

Scheme 2. Reduction of iron precursors by PhMgBr in the absence (a,b) or the presence of a hydrogen donor (c); (*) The presence of more than 100% of PhH after acidic quench is due to the presence of traces of benzene in the starting material.[13]

In order to evidence the formation of putative transient radical intermediates, radical-trapping experiments were performed using tris-(trimethylsilyl)silane (TTMSSH = $(Me_3Si)_3SiH$) as a hydrogen donor. The reduction of either $Fe(acac)_n$ or $FeCl_n$ (n = 2, 3) by an excess of PhMgBr in the presence of TTMSSH inhibits the formation of PhPh, usually observed as the sole byproduct upon oxidation of PhMgBr by Fe^{III} or Fe^{II} (Scheme 2a), and only leads to the formation of benzene (Scheme 2c). It suggests that in the absence of TTMSSH, phenyl radicals $Ph^{\bullet}$ are produced during the reduction of the Fe^{III} or Fe^{II} precursor, recombination of these radicals leading to the formation of PhPh. In the presence of a strong hydrogen donor such as TTMSSH, $Ph^{\bullet}$ is transformed into benzene by hydrogen atom transfer in a process faster than dimerization. Therefore, this shows that the monoelectronic reduction of $Fe(acac)_3$ by PhMgBr is preferred to a classic bielectronic reductive elimination from a putative bis-phenyl $(Ph)_2[Fe^{III}]$ species, which would directly yield from Fe^{III} to Fe^{I} in a radical-free process (with formation of PhPh). The possibility of a reduction involving direct single electronic transfer (SET) proceeding by outer sphere between PhMgBr and $Fe(acac)_3$ and leading to a Fe^{II} species (namely $[Fe^{II}(acac)_3]^{-}$) would be unlikely due to the high gap between the oxidation potential of PhMgBr in THF (ca. 0.0 V vs SHE[14a]) and the reduction potential of $Fe(acac)_3$ (-0.49 V vs SHE[14b]).[14c-d] DFT calculations were carried out to investigate the reduction of $Fe(acac)_3$ by inner-sphere-type electronic transfers. A coordination of $C_6H_5^{-}$, transferred from PhMgBr onto the iron center, leading to $PhFe^{III}(acac)_2$, is thermodynamically favored (exothermicity of 15.8 $kcal.mol^{-1}$, Scheme 3a). However, a second phenyl anion transfer leading to $[Ph_2Fe^{III}(acac)_2]^{-}$ requires an overall span of 27 $kcal.mol^{-1}$, precluding its formation under the reaction conditions (-30 to 25 °C) (Schemes 1, 2). This explains why bielectronic reductive elimination directly connecting Fe^{III} and Fe^{I} oxidation states does not occur here.

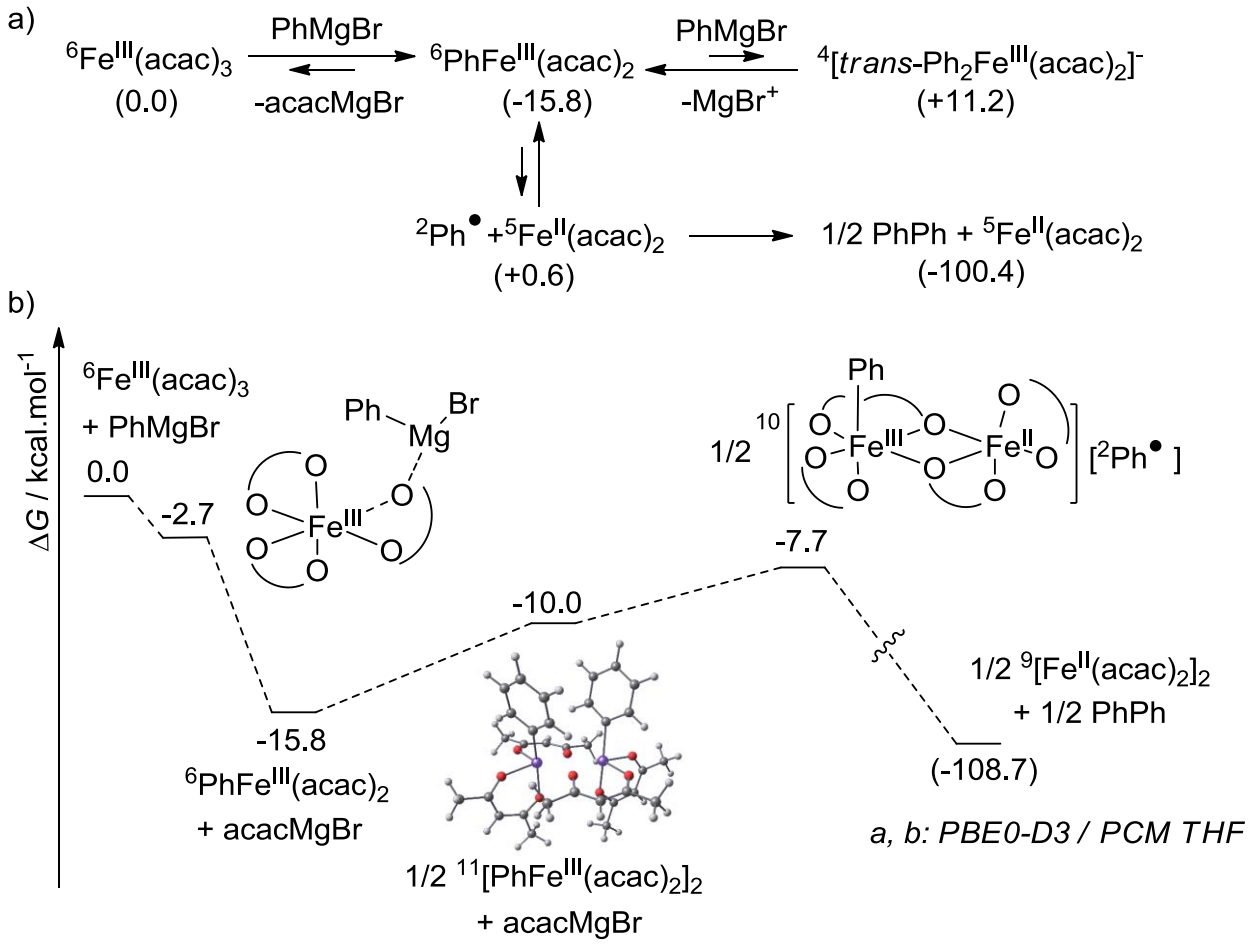

Scheme 3. computed free energies (kcal.mol^{-1}) of a) mono- and bis-phenyl-Fe^{III} intermediate formation; b) reduction of $Fe(acac)_3$ into $Fe(acac)_2$ by PhMgBr involving a dimeric process; ground spin multiplicities in superscript (solvation THF molecules omitted for clarity, see SI).

The Mg-to-Fe phenyl anion transfer described in Scheme 3a can involve the formation of an adduct exhibiting a Fe─O─Mg linkage (ΔG = -2.7 kcal.mol^{-1}, Scheme 3b), thus weakening the coordination of one of the acac$^-$ ligands. This adduct prefigures the release of acacMgBr and the formation of the C─Fe^{III} bond (computed exothermicity of -15.8 kcal.mol^{-1}). The ability of $PhFe^{III}(acac)_2$ to undergo homolytic C─Fe cleavage and generate $Fe(acac)_2$ in its ground spin state (quintet) was investigated. A global endothermicity of 16.4 kcal.mol^{-1} has been obtained

(Scheme 3a), which is incompatible with the experimental conditions (reaction time of ca. 5 minutes at rt). Moreover, the release of free $Ph^{\bullet}$ radicals in a solvent such as THF could hardly explain the quantitative formation of PhPh as a recombination product, since carboradicals can readily abstract hydrogen atoms from THF. However, it is known that $Fe(acac)_2$ can accommodate oligomeric structures, thanks to the presence of vacant coordination sites.[12] An alternative pathway involving the formation of an O(acac)-bridged dimer leading to $[Fe(acac)_2]_2$ has been computed, and allows the reduction to process with a lower energy barrier (8.1 $kcal.mol^{-1}$, Scheme 3b). In this dimeric process, phenyl radical $Ph^{\bullet}$ and Fe^{III}-bonded $C_6H_5^-$ ligand can undergo in-cage recombination to lead to the formation of PhPh. The further reduction of $Fe(acac)_2$ to lower oxidation states can then proceed, most likely *via* the formation of an intermediate organo-Fe^{II} complex, similarly to the Fe^{III} to Fe^{II} reduction route. The titration of the biphenyl obtained by the reduction of $FeCl_2$ by 30 equiv. of PhMgBr showed that upon 30 minutes at room temperature and after acidic quenching, ca. 1 equiv. of PhPh was obtained per mole of iron, which corresponds to an average transfer of 2 electrons per mole of Fe^{II} (Scheme 2b).[13]

In a previous contribution mainly focused on cyclic voltammetry,[14b] we demonstrated that chemical reduction of $Fe(acac)_3$ by PhMgBr in THF led to a mixture of Fe^{II}, Fe^{I} and Fe^{0} oxidation states depending on the PhMgBr:Fe ratio. In the presence of a moderate excess of Grignard reagent (from 9 up to 15 equiv. per mole of iron), two well-defined paramagnetic species could be characterized by their ^1H NMR spectra. Addition of a larger amount of PhMgBr (> 15 equiv. overall per mole of iron) led to a drastic alteration of the NMR spectra since no signal could be detected. This was associated with an evolution of the color of the sample which

switched from pale green to dark brown and, in these conditions, the formation of a low-spin Fe^{I} species was attested by cw-EPR spectroscopy, and the formula $[PhFe^{I}(acac)(THF)]^{-}$ was tentatively attributed. However, as highlighted by Bedford and coworkers[4], DFT-based computational analysis shows that this species exhibits a strong preference for the quartet spin state and therefore cannot account for the low-spin Fe^{I} complex detected by EPR spectroscopy. In order to investigate more closely the nature of the low-valent iron complexes obtained in these systems, we decided to examine and compare the EPR spectra of frozen solutions containing various Fe^{II} and Fe^{III} salts reduced by PhMgBr in toluene:THF (10:1) mixtures. The choice of toluene as a major co-solvent has been motivated by the fact that arene ligands often stabilize iron low oxidation states.[15]

Reduction of Fe^{II} and Fe^{III} salts monitored by EPR spectroscopy in toluene:THF (10:1). Additionally to the use of β-diketonate salts, the reduction of iron chloride precursors ($FeCl_2$ and $FeCl_3$) with PhMgBr was investigated by EPR spectroscopy. These salts are also excellent catalysts in Kumada coupling reactions.[2] They do not benefit from the presence of stabilizing $acac^{-}$ ligands and are more electron-deficient, being thus more easily reduced by PhMgBr. Unlike the reduction of $Fe(acac)_3$, the reduction of $FeCl_3$ by 1 equiv. of PhMgBr provides a mixture of a low-spin Fe^{I} complex and high-spin Fe^{III} unidentified species, as attested by EPR spectroscopy (Scheme 4 and SI). These data support the formation of transient polyphenyl-Fe^{III} species,[16] which can evolve to the formation of Fe^{I}.

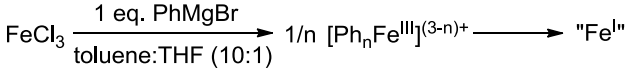

Scheme 4. Reduction of Fe^{III} into Fe^{I} by 1 equiv. PhMgBr in toluene:THF (10:1).

The comparison of the X-band EPR spectra of samples resulting from the reduction of $Fe(acac)_3$, $FeCl_2$ and $FeCl_3$ by a large excess of PhMgBr (30 equiv.) carried out at room temperature (reaction time : 2 minutes) shows that the same S = 1/2 species is formed, with g-values of 2.21, 2.02 and 2.00 (see Figure 1 for the case of $FeCl_2$, see SI for the spectra recorded using $FeCl_3$ and $Fe(acac)_3$ as precursors). Interestingly, a similar EPR spectrum exhibiting very close g-values (g = 2.20, 2.02 and 1.99) was obtained when the reduction of $Fe(acac)_3$ was carried out in pure THF.[14b] This signal is characteristic of a S = 1/2 transition-metal-based system with resolved g-anisotropy, and is consistent with the formation of a low-spin mononuclear Fe^I species. Moreover, the three g-values are in good agreement with other reported EPR data for similar Fe^I low-spin mononuclear systems (Table 1).[6a,17]

Table 1. Selection of EPR g-values for low-spin Fe^I mononuclear complexes.

Entry	Complex	g-values	Ref.
1	(p-tolyl)(1,2-$C_6H_4(PPh_2)_2)_2$Fe	2.25 / 2.09 / 2.08	[6a]
2	(η^6-C_6H_6)(NacNac)Fe (*)	2.20 / 2.01 / 1.98	[17a]
3	Na(trop$_2$dae)$(THF)_3$Fe (**)	2.16 / 2.06 / 2.01	[17b]

(*) NacNac = HC(C[Me]N-(2,6-diisopropylphenyl))$_2$; (**) trop=5*H*-dibenzo[*a*,*d*]cyclo-hepten-5-yl, dae=(N-CH_2-CH_2-N).

The obtention of the same spectra regardless of the nature of the precursor implies that all the $acac^-$ ligands are displaced in the bielectronic reduction of $Fe(acac)_3$. A redistribution of the $acac^-$ and Ph^- ligands is indeed observed, the harder ligand ($acac^-$) being transferred from Fe to Mg, and the softer ligand ($C_6H_5^-$) being transferred from Mg to Fe: [*trans*-$(THF)_2Mg(acac)_2]\mu^2$(O,O)$FeBr_2$ was obtained at –30°C and characterized by single-crystal X-Ray diffraction.[18] When a Fe^{II} salt is used as a precursor, an alternative mechanism for the

generation of the Fe^{I} oxidation state can be evidenced. The reduction of $FeCl_2$ by 30 equiv. of PhMgBr provided a mixture containing a well-defined Fe^{I} species and high-spin Fe^{III} complexes as attested by EPR spectroscopy (Figure 1). This shows that Fe^{I} and Fe^{III} oxidation states can be provided by a fast disproportionation process of intermediate polyphenyl-Fe^{II} complexes.[19a] A similar hypothesis was formulated by Bedford et al., who reported that benzylic ate-complex $[Fe^{II}(benzyl)_3]^-$ yields Fe^{III} and Fe^{I} species by a disproportionation pathway.[19b] Koszinowski et al. also reported that $[Ph_4Fe^{III}]^-$ and $[Ph_3Fe^{II}]^-$ could be detected concomitantly by ESI-MS when Fe^{II} *in-situ*-generated species reacted with an excess of PhMgCl.[19c]

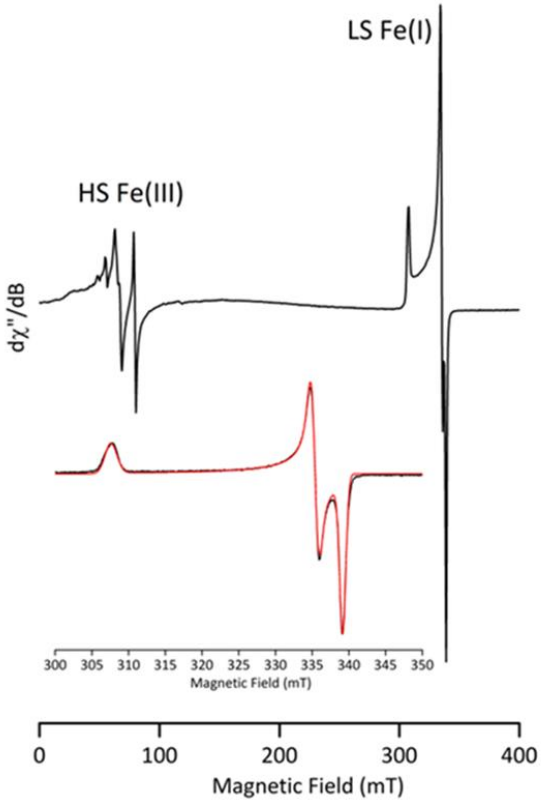

Figure 1. cw-EPR spectrum (h_8-toluene:h_8-THF 10:1 glass) of $FeCl_2$ + 30 equiv. PhMgBr (frozen after 2 minutes at 25°C). Inset: spectrum under non saturating conditions of the g = 2 region (Fe^{I} species, black: exp., red: simul.). Experimental conditions: microwave frequency

9.50 GHz; microwave power 1 mW and 0.25 mW (inset); field modulation amplitude 1 mT and 0.25 mT (inset); field modulation frequency 100 kHz; T = 10 K and 60 K (inset). Simulation parameters: g = 2.2059, 2.0230 and 2.0003, H_{strain} (MHz) = 50.5; 15.8 and 0.0, linewidth 1 MHz.

A quantitation of the Fe^{I} species obtained by double integration of its EPR signal and comparison with standard solutions of $CuSO_4$ recorded under the same non-saturating conditions demonstrated that after a reaction time of 2 minutes at room temperature (Figure 1), the Fe^{I} species represents about 15% of the overall iron quantity. This indicates that the most important part of the metal is under other forms or oxidation states, including EPR-silent species.

Stability of the Fe^{I} oxidation state. It is noteworthy that the Fe^{I} complex formed upon reduction of $FeCl_2$ by PhMgBr proved to be unstable over time. Indeed, a second minor complex is sometimes observed after 5 min at room temperature (Figure 2a, black, g_{max} = 2.22). After 24 h at room temperature, the overall Fe^{I} quantity only represents 20% of the starting Fe^{I} quantity detected in EPR (Figure 2a, blue, g_{max} = 2.20, 2.21 and 2.22). The system evolves towards the formation of clusters, potentially nanoparticles, as suggested by new broad EPR resonances observed (Figure 2b) over a wide range of magnetic field values (1 T).

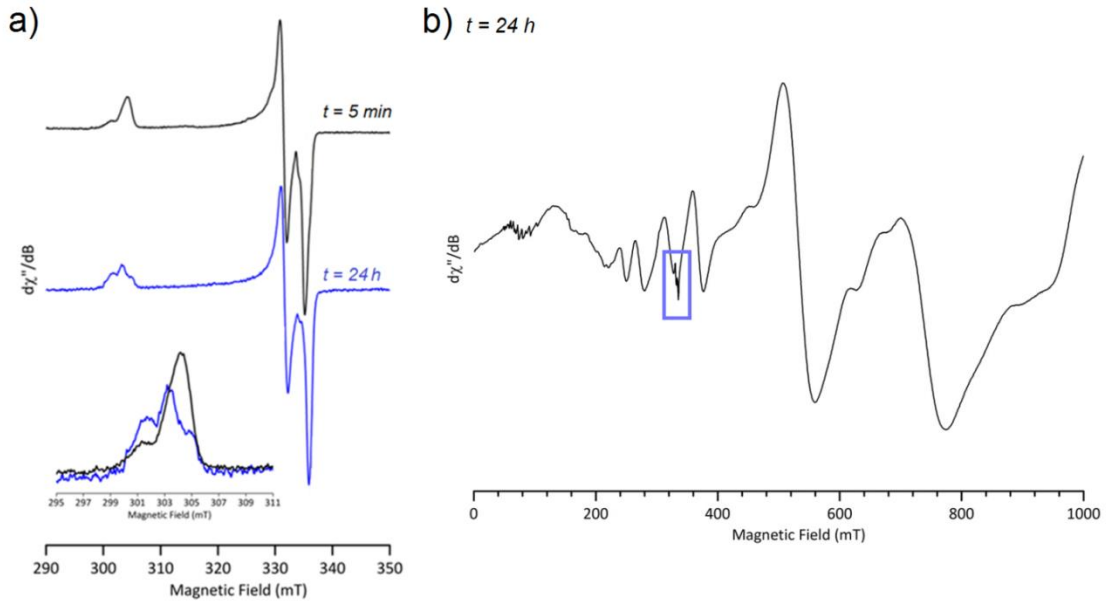

Figure 2. a) cw-EPR spectrum (h_8-toluene:h_8-THF 10:1 glass) of $FeCl_2$ + 30 equiv. PhMgBr frozen after 5 min (black; vertical scale: 1/1) or 24 h (blue; vertical scale: 5/1) at 298 K, inset: zoom on the g_{max} area; experimental conditions : microwave frequency 9.40 GHz; microwave power 0.06 mW (blue) and 0.02 mW (black); field modulation amplitude 0.5 mT (blue) and 0.2 mT (black); field modulation frequency 100 kHz; temperature 50 K; b) wide field range spectrum of the 24 h sample; experimental conditions: microwave frequency 9.40 GHz; microwave power 1 mW; field modulation amplitude 0.5 mT; field modulation frequency 100 kHz; temperature 10 K.

The evolution of the intensity of the Fe^{I} signal in EPR spectroscopy clearly shows that this complex is unstable over time. Importantly, the EPR spectrum recorded after 24 h suggests that the system evolved towards paramagnetic clusters. In order to investigate the formation and the fate of the EPR-silent integer spin species, the reduction of isotopically-enriched $^{57}Fe^{II}$

precursors was investigated by Mössbauer spectroscopy, thus allowing an overview of the whole distribution of iron oxidation states reached in these systems.

Mössbauer spectroscopy investigations. Since bromine atoms strongly absorb γ radiations and are thus highly detrimental to the quality of Mössbauer spectra, we investigated the reduction of isotopically-enriched $^{57}FeCl_2$ with an excess (30 equiv.) of PhMgCl in toluene:THF (10:1) during 3 min, inside an inert atmosphere box. Mössbauer spectra of the frozen sample (Figure 3) were recorded at low temperatures (4.2 to 20 K) in absence (Figure 3a) or in presence (Figure 3b-c) of a high magnetic field (7T) applied parallel to the γ rays. In order to circumvent as efficiently as possible the fast formation of iron aggregates in the reduction process, spectra have been run at low ^{57}Fe concentration (2.5 mM).

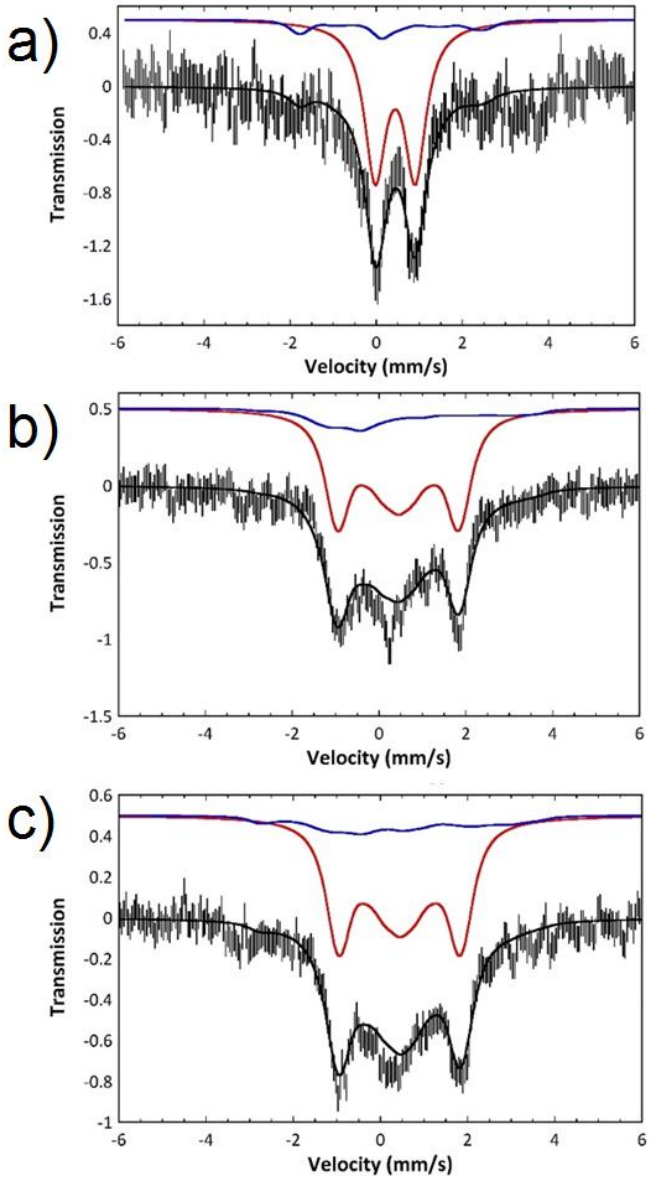

Figure 3. Mössbauer spectra of frozen solutions resulting from the reduction of $^{57}FeCl_2$ in toluene:THF by PhMgCl (30 equiv.; overall ^{57}Fe concentration: 2.5 mM) after 3 minutes at room temperature; a) T = 5 K, no magnetic field; b) T = 4.2 K, 7 T; c) T = 20 K, 7 T. The low signal-to-noise ratio is due to the diluted conditions (2.5 mM $^{57}FeCl_2$) as well as to the large excess of chloride anions.

In absence of applied field the spectrum appears as a broad quadrupole doublet and a similar doublet was observed at 80 K. Application of a magnetic field splits the doublet over a small velocity range (-1 to +2 $mm.s^{-1}$). This is a typical behavior of a spin S = 0 system and all spectra could be simulated under this assumption with the following nuclear parameters: δ = 0.44 $mm.s^{-1}$ and ΔE_Q = 0.93 $mm.s^{-1}$. This simulation accounts for ca 85 % of the iron present in the sample (Figure 3, red lines). However, it does not totally reproduce parts of the spectrum on both sides of the central multiplet (velocity domains -4 to -3 and 3 to 4 $mm.s^{-1}$). Moreover these features are both field and temperature dependent (increase at 20 K). This suggests the occurrence of a minor additional species with a half-integer spin. The whole spectrum could be simulated by considering that the sample is a mixture of a spin S = 0 species and a spin S = 1/2 species (Figure 3, blue lines) using the g values deduced from the EPR experiment and literature hyperfine values (Table 2).[20] The nuclear parameters for this paramagnetic species are δ = 0.28 $mm.s^{-1}$ and ΔE_Q = 2.01 $mm.s^{-1}$. Owing to the low signal to noise ratio of the spectrum and the intrinsic similarity of the spectra of both components, a precise determination of their respective contributions is not achievable; however, the content of the S = 1/2 species can be estimated within the range 10 to 20 %. Mössbauer experiments are thus fully consistent with the EPR analysis pointing to the formation of a major S = 0 species (EPR silent) and a minor S = 1/2 species. The nuclear parameters of the major Fe center are not unambiguous, as is often the case for low spin systems, and could be associated to Fe^{II},[8] Fe^{I},[21] or Fe^0 species.[22] However, the formation of the Fe^0 oxidation state as a major species is consistent with the overall transfer of 2 electrons per iron ion (vide supra). In addition, the nuclear parameters of the diamagnetic species evidenced herein (δ = 0.44 $mm.s^{-1}$, ΔE_Q = 0.93 $mm.s^{-1}$) are similar to those published for related arene-stabilized Fe^0 species: (η^6-C_6H_6)(η^4-C_6H_8)Fe^0 (δ = 0.51 $mm.s^{-1}$, ΔE_Q = 0.94 $mm.s^{-1}$) and

(η^6-C_6H_6)(η^4-C_6H_6)Fe^0 (δ = 0.64 mm.s^{-1}, ΔE_Q = 1.04 mm.s^{-1}).[22a] It moreover echoes the report of Neidig who showed that the reduction of SciOPP-stabilized Fe^{II} precursors by PhMgBr led at room temperature to a similar diamagnetic Fe^0 arene-stabilized species (η^6-biphenyl)Fe^0(SciOPP) with a close isomer shift and a higher quadrupolar split (δ = 0.44 mm.s^{-1}, ΔE_Q = 1.75 mm.s^{-1}).[8] It is interesting to note that the high-spin Fe^{III} species detected in EPR spectroscopy (Figure 1) were not detected in Mössbauer spectroscopy, which shows that the overall concentration of Fe^{III} is significantly smaller than Fe^I. On this basis, it can be suggested that the most important part of Fe^I species is not formed by the disproportionation of polyphenyliron(II) intermediates.

Table 2. Best-fit parameters deduced from the simulation of the Mössbauer spectra (see Figure 3 and SI) taking into account a mixture of S = 0 (Fe^0) and S = 1/2 (Fe^I) species using the experimental EPR g-values reported herein and nuclear hyperfine values consistent with literature data.[20]

Entry	Iron ox. state	Spin	$g_{x,y,z}$	δ (mm.s^{-1})	ΔE_Q (mm.s^{-1})	Γ (mm.s^{-1})	η	A_x (T)	A_y (T)	A_z (T)	% ± 5%
1	Fe^0	0	-	0.44	0.93	0.60	0.97	-	-	-	85
2	Fe^I	1/2	2.21 (g_x) 2.02 (g_y) 2.00 (g_z)	0.28	2.01	0.48	0.63	19	13	18	15

Stabilization of "elemental iron atoms" at the zero oxidation state by arene and alkene neutral ligands (leading e.g. to (η^6-arene)(η^4-diene)Fe^0 complexes) has been already reported in the past.[22,23,24] These molecular species can be obtained by reducing bis-arene-ligated Fe^{II} precursors with monoelectronic reductants such as sodium amalgam[23] or by co-condensing elemental iron

atoms and organic ligands onto low-temperature frozen surfaces.[24] Three different modes of coordination can be accommodated by Fe^0 centers in the presence of arene ligands depending on their hapticity. This can lead to the formation of 20-electron (Scheme 5a), 18-electron (Scheme 5b) or 16-electron (Scheme 5c) species.

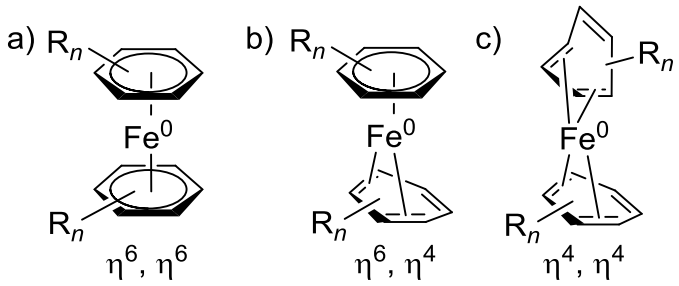

Scheme 5. Possible coordination modes (η^6- or η^4-) of Fe^0 atoms by arene ligands.

Binding modes of the arene ligand strongly depend on the nature of both the arene and the temperature. Astruc et al. demonstrated by Mössbauer spectroscopy that the reduction of Fe^{II} to the Fe^0 oxidation state in mesitylene led to the formation of the bis-η^6 corresponding adduct (η^6-$C_6Me_6)_2Fe^0$ (Scheme 5a, R = Me_6).[23] It has been shown by low-temperature metal atom matrix UV-visible and IR investigations that iron atoms condensed in benzene vapor led to the formation of the 18-electron complex (η^6-C_6H_6)(η^4-C_6H_6)Fe^0 (Scheme 5b, R = H_6) as the sole product (in the range of T = 50 to 240 K).[22a,24b] On the other hand, iron atoms condensed in toluene vapor could exhibit two coordination modes. A 18-electron (η^6-C_6H_5Me)(η^4-C_6H_5Me)Fe^0 complex is favored at medium temperatures (90 to 240 K, Scheme 5b, R = Me), whereas a 16-electron complex (η^4-$C_6H_5Me)_2Fe^0$ is obtained at lower temperatures (< 77 K, Scheme 5c, R = Me).[24b] Both complexes lead to the formation of clusters upon warming. In our case, it seems unlikely that a bis-η^6-toluene coordinated Fe^0 complex is obtained since the analogue species (η^6-$C_6Me_6)_2Fe^0$ and (η^6-$C_6H_6)_2Fe^0$ exhibit much higher isomer shifts (resp. 1.06

mm.s^{-1} and 1.22 mm.s^{-1}) and higher quadrupolar splits (resp. -1.45 and 1.84 mm.s^{-1}).[22a,23] More specifically, it has been demonstrated by Mössbauer spectroscopy that (η^6-C_6Me_6)$_2$Fe^0 accommodated a spin triplet state (S = 1).[23] This is in stark contrast with the electronic structure of the Fe^0 complex discussed here, which is a singlet spin state (Figure 3). The possibility of the formation of bis-toluene (η^6,η^4)- or (η^4,η^4)-ligated Fe^0 complexes has been further investigated by theoretical modellings.

Analysis of the Mössbauer spectra: insights from DFT calculations. Mössbauer parameters can indeed be easily evaluated using straightforward DFT techniques, which allow the computation of the electronic density at the ^{57}Fe nucleus, noted ρ_0 (unit: e.a_0^{-3}, where a_0 is Bohr radius). A reliable estimation of the isomer shift (δ) can thus be obtained with a linear extrapolation from ρ_0.[25a] To do so, a benchmark of Fe^0 and Fe^I complexes[25b,c] has been used to calibrate the chosen level of theory. All calculations were performed with ORCA 3.0.3 software, using the BP86 functional in gas phase, associated with the TZVP basis set for all atoms except Fe which was treated with the CP(PPP) enlarged basis set. This choice has been motivated since it allows a good compromise between accuracy and computational time. It has indeed been demonstrated that the use of CP(PPP) basis set on iron allowed more accurate linear fit between ρ_0 and δ for a very modest additional computational cost.[25a]

The level of theory used in this benchmark allowed us to compute the isomer shift of the already reported complexes (η^6-C_6Me_6)$_2$Fe^0, (η^6-C_6H_6)(η^4-C_6H_6)Fe^0, and (η^6-C_6H_6)(η^4-C_6H_8)Fe^0 with a good accuracy (Table 3, entries 1-3). For model complexes involving η^4 toluene-coordinated species, the position of the Me group (borne by C_1 atom) in the η^4-ligand did not have significant

impact on either the calculated isomer shift or the average Fe─C_{arene} distances; see Table 3, entries 4 (η^4-$C_1C_2C_3C_4$), 5 (η^4-$C_1C_2C_3C_6$) and 6 (η^4-$C_2C_3C_4C_5$). It can be noted that these species exhibit isomer shifts very close to their bis-C_6H_6 analogue (Table 3, entry 2).

Table 3. Calculated and observed isomer shifts (δ) for several bis-arene or bis-diene Fe^0 complexes.

Entry	Complex	Spin	ρ_0 (calcd.) ($e.a_0^{-3}$)	δ (calcd.) ($mm.s^{-1}$)	δ (expt.) ($mm.s^{-1}$)	Ref.
1	$(\eta^6\text{-}C_6Me_6)_2Fe^0$	1	11826.87	0.99	1.06	[23]
2	$(\eta^6\text{-}C_6H_6)(\eta^4\text{-}C_6H_6)Fe^0$	0	11827.85	0.58	0.64	[22a]
3	$(\eta^6\text{-}C_6H_6)(\eta^4\text{-}C_6H_8)Fe^0$	0	11827.87	0.57	0.51	[22a]
4	$(\eta^6\text{-}C_6H_5Me)(\eta^4\text{-}C_6H_5Me)Fe^0$	0	11827.83	0.59	-	-
5	$(\eta^6\text{-}C_6H_5Me)(\eta^4\text{-}C_6H_5Me)Fe^0$	0	11827.88	0.57	-	-
6	$(\eta^6\text{-}C_6H_5Me)(\eta^4\text{-}C_6H_5Me)Fe^0$	0	11827.85	0.58	-	-
7	$(\eta^4\text{-}CH_2CMeCHCH_2)_2Fe^0$	0	11828.35	0.38	-	-
8	$(\eta^4\text{-}C_6H_5Me)_2Fe^0$	0	11828.04	0.50	-	-

A noticeable trend which can be drawn from this computational analysis is that the average Fe─C_{arene} bond is slightly longer for η^6-coordinated arene ligands than for their η^4 analogues. In the case of $(\eta^6\text{-}C_6H_5Me)(\eta^4\text{-}C_6H_5Me)Fe^0$ (Table 3, entries 4-6) the average computed Fe─$C_{\eta 6\text{-}arene}$ distance is 2.11 Å, whereas the average Fe─$C_{\eta 4\text{-}arene}$ distance is 2.06 Å. This trend is confirmed by the optimized structure of the model complex $(\eta^4\text{-}CH_2CMeCHCH_2)_2Fe^0$ (Table 3, entry 7), which features an average Fe─$C_{\eta 4\text{-}diene}$ distance close to 2.04 Å. A smaller Fe─C_{sp2} distance leads to a higher computed electronic density ρ_0, and, therefore, to a smaller computed

isomer shift (0.38 mm.s^{-1} for (η^4-$CH_2CMeCHCH_2$)$_2$Fe^0 (entry 7) vs. 0.57-0.59 mm.s^{-1} for (η^6-C_6H_5Me)(η^4-C_6H_5Me)Fe^0 (entries 4-6)). Taking this into account, the analysis of the bis-η^4 complex (η^4-C_6H_5Me)$_2$Fe^0 nuclear parameters was performed. The computed electronic density ρ_0 was significantly higher (11828.04 e.a_0^{-3}, entry 8) than for the (η^6-C_6H_5Me)(η^4-C_6H_5Me)Fe^0 complexes (entries 4-6), and the corresponding isomer shift (0.50 mm.s^{-1}) is in good agreement with the experimentally observed data (δ = 0.44 mm.s^{-1}, Figure 3). It must be stated that the two η^4-coordinated toluene ligands do not play a symmetric role: one of them is strongly twisted, whereas the second one is almost planar (Scheme 6). The η^4-coordination onto the planar toluene is due to a displacement of the iron atom, which is slightly shifted from the pseudo C_6-symmetry axis of the η^6 ligand.

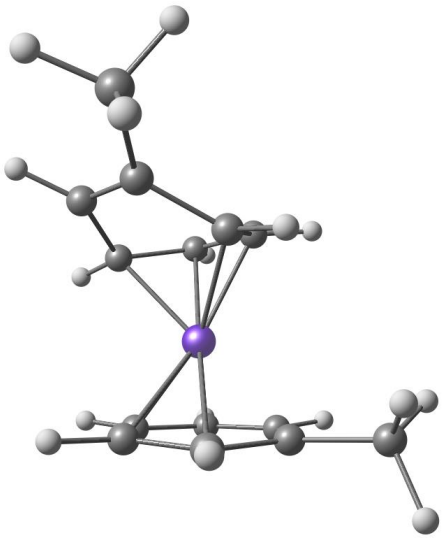

Scheme 6. Computed structure of (η^4-C_6H_5Me)$_2$Fe^0, suggested as a model for the diamagnetic Fe^0 species detected in Figure 3. Selected metric data for the η^4-($C_2C_3C_4C_5$) toluene moiety : Fe─C_1 = 2.15 Å; Fe─C_2 = 2.08 Å; Fe─C_3 = 1.95 Å; Fe─C_4 = 1.95 Å; Fe─C_5 = 2.08 Å; Fe─C_6 = 2.14 Å; Fe─C_n bonds (n = 2-5) frozen during the optimization.

Suggestion of a bis-arene-ligated Fe^0 species as a major complex obtained in the conditions depicted above (reduction of FeX_n salts by 30 equiv. PhMg(Hal), 2 min. in toluene) is therefore in good agreement with the literature[24b] and with the Mössbauer spectroscopy analysis reported herein (using $^{57}FeCl_2$ as a precursor). This species evolves towards the formation of paramagnetic aggregates as evidenced by the strongly distorded EPR spectrum in Figure 2b. However, the computed isomer shift δ is extremely sensitive to the Fe─C_{arene} bond distances and consequently to the theoretical level applied (δ variation of more than 30% for less than 5% of difference between the average Fe–C_{arene} distances in the structures depicted in Table 3, entries 4-6 and 8). Therefore, care must be taken in the interpretation of the experimental data, especially due to the low signal-to-noise ratio of the spectra displayed in Figure 3. An average error of ± 0.05 $mm.s^{-1}$ on the simulation of the nuclear parameters should be acknowledged. Consequently, it can be anticipated that several geometrically close species featuring arene-ligated Fe^0 centers which could fall in this error range co-exist in solution.

^{1}H NMR spectroscopy. The formation of transient arene-coordinated Fe^0 species was also suggested by ^{1}H NMR spectroscopy when $Fe(acac)_3$ was used as a precursor in d_8-toluene. At low iron concentrations (0.7 mM) and low temperature (-40°C), reduction of $Fe(acac)_3$ by PhMgBr (50 equiv.) in the presence of PhPh as an additive (50 equiv. of which were added to ensure the presence of a large excess of arene ligands in the bulk) led to the observation of transient resonances in the 4-5 ppm area (δ = 5.00, 4.72, 4.45, 4.31 and 4.15 ppm, see SI). Such resonances are usually observed in this range for diamagnetic Fe^0 arene-coordinated species, arene protons being upfielded by retrodonation from the metal: Ittel et al. reported that the arene protons resonances of the analogue complex (η^6-toluene)Fe^0(butadiene) were observed between

4.66 and 4.87 ppm.[24a] The number of resonances observed in our conditions (vide supra) also suggests that multiple arene-coordinated Fe^0 species are obtained in the bulk upon chemical reduction of the precursor by PhMgX (X = Cl, Br). Consistently with the evolution of these Fe^0 complexes towards paramagnetic aggregates, the resonances described above quickly disappeared. The only ^1H NMR signals observed after 10 minutes at -40°C or upon slow warming at room temperature in the 4-6 ppm area belonged to the free $acac^-$ ligand (δ = 5.25 ppm, CH), which was released in the reduction process (Scheme 2a). Concomitantly, the color of the solution evolved from very pale red-brown to a deep dark brown.

The nature of the minor Fe^I complex evidenced in EPR and Mössbauer spectra (Figures 1 and 3) is discussed in the next section. As evidenced by spin titration in both the aforementioned techniques, this oxidation state only represents a small fraction of the overall iron quantity (ca. 15%).

Nature of the Fe^I complex: insights from pulsed-EPR spectroscopy. In order to investigate the nature of the Fe^I coordination sphere, pulsed-EPR experiments (HYSCORE) were realized in toluene:THF (10:1) glass. HYSCORE is a powerful 2D pulse EPR technique that allows the study of the hyperfine couplings of nuclei coupled to the paramagnetic species of interest. Figure 4 shows the HYSCORE quadrant plots obtained for magnetic field values corresponding to the three principal g-values of the Fe^I complex. Here, ridges well separated from the ^1H Larmor frequency are observed and extend over nearly 12 MHz, indicating specific proton coupling to the Fe^I ion. These ridges disappear when the same experiments are performed in fully deuterated toluene (associated with 10% h_8-THF, see SI) indicating that the signals can be attributed to the

protons of the toluene solvent in close interaction with the metal ion. Therefore, the signals observed are compatible with a toluene molecule in a η^6-coordination to Fe^I. The strong affinity of low-valent iron ions for arene ligands is already known (vide supra) and several well-defined arene-coordinated Fe^I complexes have been reported and for some of them investigated with spectroscopic and theoretical methods.[17a,26a]

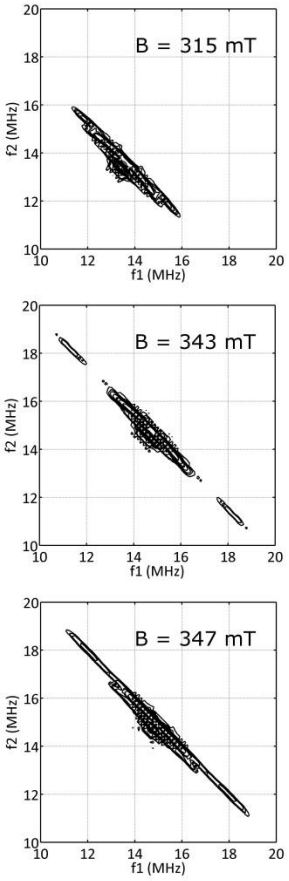

Figure 4. HYSCORE contour plots for Fe^I ($FeCl_2$ + 30 equiv. PhMgBr; h_8-toluene:h_8-THF 10:1 glass) at g_{max} (315 mT), g_{mid} (343 mT) and g_{min} (347 mT). Experimental parameters: microwave frequency 9.71 MHz, τ = 120 ns, shot repetition time 5 ms, T = 10 K.

HYSCORE experiments performed in deuterated toluene, unambiguously show that the arene coordination of the Fe^I species implies the ligation of a toluene molecule and not a biphenyl

progressively formed in the bulk by oxidation of the Grignard reagent. However, it cannot be excluded that biphenyl acts as a η^6-coordinating arene ligand in other solvents, e.g. when the reduction is carried out in THF. The competition between the iron coordination by toluene and biphenyl is discussed at the end of the next section.

Based on cw-EPR and HYSCORE experiments, it is thus reasonable to suggest that a η^6-arene-stabilized Fe^I species is formed upon reduction of the iron precursor by PhMgBr. The nature of the other ligands of the coordination sphere was then investigated. Fe^I complexes often feature strongly σ-donating ligands, such as β-diketiminate[17a], NHCs[21b], aryl groups[26a] or trimethylsilylamides[26b]. In the presence of strongly coordinating species such as the $C_6H_5^-$ anion, it is likely that the Fe^I center is coordinated by anionic phenyl ligands. To investigate this hypothesis, the reduction of $FeCl_2$ was carried out using isotopically enriched $^{13}C_6H_5MgBr$, synthesized at a microscale from commercial $^{13}C_6H_5Br$. The cw-EPR spectrum obtained for the reduction of $FeCl_2$ by 30 equiv. $^{13}C_6H_5MgBr$ during 2 minutes at room temperature is shown in Figure 5. The resonances are centered on the same g-values observed when $FeCl_2$ was reduced with non-enriched C_6H_5MgBr (Figure 1) but exhibit significant broadening reflecting hyperfine couplings between the Fe^I ion and ^{13}C nuclei.

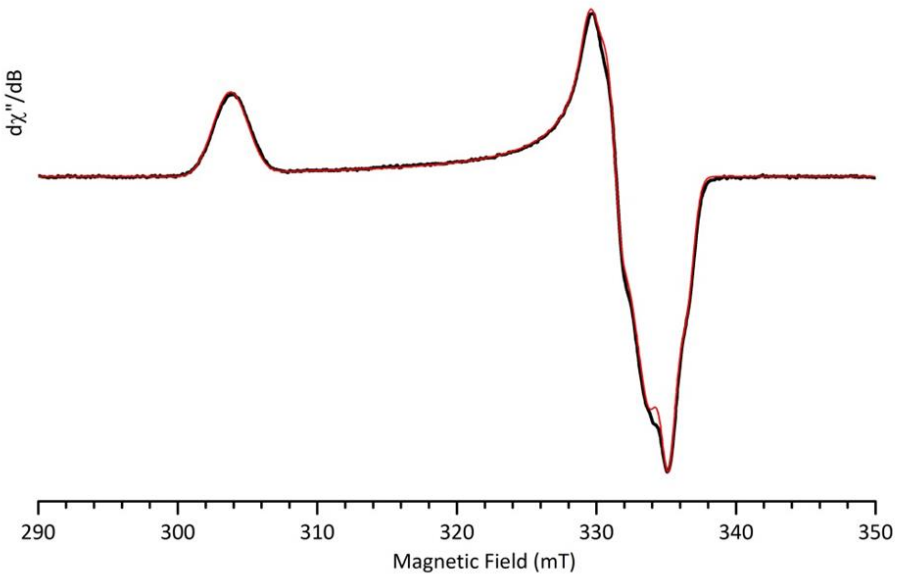

Figure 5. Experimental (black) and simulated (red) cw-EPR spectrum (*h*$_8$-toluene:*h*$_8$-THF 10:1 glass) of $FeCl_2$ + 30 equiv. $^{13}C_6H_5MgBr$. Experimental parameters: microwave frequency 9.38 GHz; microwave power 0.01 mW; field modulation amplitude 0.5 mT; field modulation frequency 100 kHz; temperature 50 K. Simulation parameters: g = 2.2059, 2.0230 and 2.0003, H_{strain} (MHz) = 50.5, 15.8 and 0.0, linewidth 1 MHz, 2 equivalent ^{13}C nuclei with A_{iso} = 35 MHz and 4 equivalent ^{13}C nuclei with A_{iso} = 9.0; 8.8 and 9.2 (in MHz).

Since the coupling is not resolved on the cw-EPR spectrum, we performed HYSCORE measurements on this sample. The contour plots obtained at magnetic field values corresponding to the principal g-values are shown in Figure 6. Signals were observed in both quadrants, corresponding to strong and weak coupling cases. The cross peaks in the (+–) quadrant do not exhibit significant changes in their position suggesting that the hyperfine coupling of the corresponding ^{13}C nuclei is essentially isotropic. Based on the distance between the cross-peaks, the value of the coupling was estimated to be about 9 MHz. The fact that the coupling is isotropic indicates that some spin density is localized on ^{13}C nuclei and therefore that at least one

$^{13}C_6H_5^-$ anion is a ligand to the Fe^I ion. In the (++) quadrant, the cross peaks are not resolved and close to the ^{13}C Larmor frequency indicating rather weak hyperfine coupling.

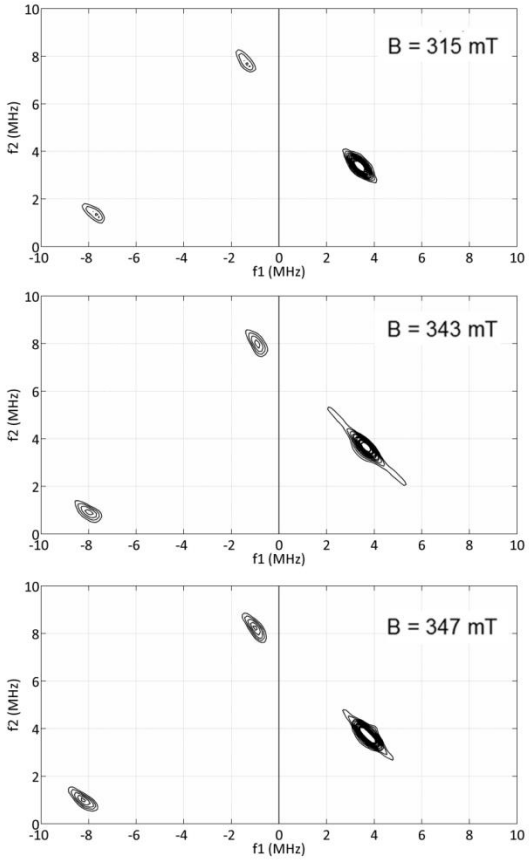

Figure 6. HYSCORE contour plots of $FeCl_2$ + 30 equiv. $^{13}C_6H_5MgBr$ (h_8-toluene:h_8-THF 10:1 glass) at g_{max} (315 mT), g_{mid} (343 mT) and g_{min} (347 mT). Experimental parameters: microwave frequency 9.71 MHz, τ = 140 ns, shot repetition time 3 ms, T = 10 K.

Based on these results, it can be proposed that the carbon bonding the Fe^I ion (C_{ipso}) bears the strongest spin density in the $C_6H_5^-$ ligands. It is therefore quite strongly coupled to the iron and not detectable by HYSCORE. This is in agreement with the simulated spectrum depicted in Figure 5 that includes a parameter A_{iso} = 35 MHz (red lines). The two carbon atoms in ortho position are those responsible for the cross-peaks observed in the (+–) quadrant with an

hyperfine coupling of 9 MHz and the carbon atoms in meta and para positions are very weakly coupled and detected close to the ^{13}C Larmor frequency in the (++) quadrant. With this in mind, simulations were performed for the cw-EPR spectrum of the sample. Keeping the same parameters (g-values, strain and linewidth) as for the spectrum without ^{13}C labelling (Figure 1, inset), the best fit was obtained when considering two equivalent $C_6H_5^-$ ligands compared to only one (see SI). The simulation is shown in Figure 5 with the experimental data and the parameters reported in the caption. The overall results obtained with cw- and pulsed-EPR thus allow suggesting the structure which is represented in Scheme 7 for the S = 1/2 Fe^I complex, namely $[(\eta^6\text{-}C_6H_5Me)Fe^I(Ph)_2]^-$.

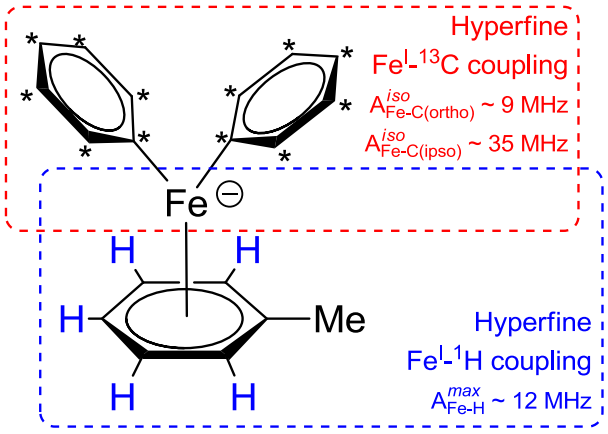

Scheme 7. Structure suggested for the minor Fe^I complex obtained by reduction of FeX_n (X = acac, Cl; n = 2, 3) by an excess of PhMgBr in toluene, on the basis of cw- and pulsed-EPR experiments; the starred atoms correspond to ^{13}C atoms which allowed the detection of the hyperfine Fe^I—^{13}C couplings when $^{13}C_6H_5MgBr$ was used as a reductant.

In order to support the structure suggested above (Scheme 7), the most likely number of $C_6H_5^-$ ligands, and, therefore, the most likely topology which can be accommodated by the Fe^I center to

afford a spin doublet arene-ligated (poly)phenyl-Fe^{I} complex $[(\eta^6\text{-}C_6H_5Me)Fe^{I}(Ph)_n]^{(n-1)-}$, was then examined using DFT calculations.

Theoretical investigations of the Fe^{I} electronic structure. The doublet-quartet spin gap was evaluated for a benchmark of representative Fe^{I} organometallic complexes reported in the literature and featuring for some of them η^6-arene-coordinated Fe^{I} centers (**1a**, **1b**, **1c** and **1d**, Scheme 8)[27]. Benzene has been used as a model for the coordinated arene solvent in each case. Different dispersion-fitted functionals were used (PBE0-D3, B3LYP-D3 and M06), as well as two pseudo-potentials for the iron ion (SDD and CEP-31G). The complexes $[(\eta^6\text{-}C_6H_6)Fe^{I}(Ph)_2]^{-}$ (**1e**) and $[(\eta^6\text{-}C_6H_6)Fe^{I}(Ph)_3]^{2-}$ (**1f**) have been used as models of η^6-arene-coordinated polyphenyl-Fe^{I} complexes exhibiting respectively idealized C_{2V} and C_{3V} environments, in order to be compared with **1d**, a bulkier terphenyl analogue of which having been experimentally characterized as a quartet spin ground state.[26a]

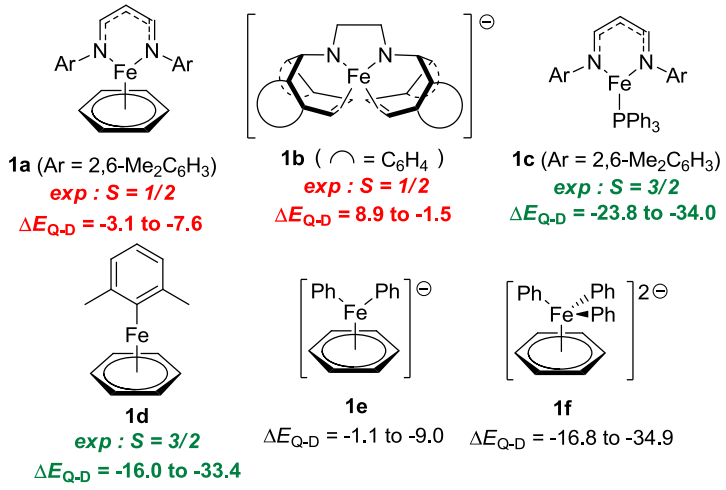

Scheme 8. $\Delta E_{Q\text{-}D} = E_Q\text{-}E_D$ DFT quartet-doublet split (kcal.mol^{-1}, gas-phase, see SI for the assignations) for **1a**, **1b**, **1c**, **1d**, **1e** and **1f**; basis sets for C, H, N, P : see SI.

Regarding the energetic features, the DFT methods reproduce well the stabilization of the quartet states (**1c** and **1d**), with a significantly high quartet-doublet gap (23.8-34.0 kcal.mol^{-1}, **1c**, and 16.0-33.4 kcal.mol^{-1}, **1d**). However, the stabilization of doublet states is not efficiently reflected by DFT analysis. All methods returned a ground quartet state for complex **1a** (stabilized by 3.1 to 7.6 kcal.mol^{-1}). Either a slight preference is returned for the doublet state for **1b** (by 2.2 to 8.9 kcal.mol^{-1}, PBE0-D3 and B3LYP-D3), or a slight preference for the quartet state (by 1.4 to 1.5 kcal.mol^{-1}, M06). Moreover, NBO analysis shows that natural orbital occupancies numbers (NOONs) for the d-block MOs strongly differ from integers (0, 1 or 2) for the computed Fe^{I} complexes (Table 4). The computed NOONs for Fe^{I} complexes **1a**, **1b**, **1c**, **1d**, **1e** and **1f** (entries 1-6) can be compared with the computed NOONs for $Fe(acac)_3$ (entry 7). The latter is essentially monoconfigurational (high spin d^5 complex) and its electronic structure is therefore accurately described by DFT.

Table 4. DFT-computed Natural Orbital Occupancies Numbers (NOONs) for d-block orbitals of complexes depicted in Scheme 8 (PBE0, gas phase, SDD and pseudopotential for Fe).

Entry	Complex	d-NOONs
1	^{2}**1a**	$d_{xy}^{1.73}d_{xz}^{0.81}d_{yz}^{1.20}d_{x2-y2}^{1.79}d_{z2}^{1.93}$
2	^{2}**1b**	$d_{xy}^{1.47}d_{xz}^{0.86}d_{yz}^{1.29}d_{x2-y2}^{1.32}d_{z2}^{1.78}$
3	^{4}**1c**	$d_{xy}^{1.27}d_{xz}^{1.60}d_{yz}^{1.57}d_{x2-y2}^{1.31}d_{z2}^{1.09}$
4	^{4}**1d**	$d_{xy}^{1.14}d_{xz}^{1.17}d_{yz}^{1.73}d_{x2-y2}^{1.31}d_{z2}^{1.64}$
5	^{2}**1e**	$d_{xy}^{0.97}d_{xz}^{1.61}d_{yz}^{1.08}d_{x2-y2}^{1.78}d_{z2}^{1.62}$
6	^{4}**1f**	$d_{xy}^{1.14}d_{xz}^{1.37}d_{yz}^{1.26}d_{x2-y2}^{1.30}d_{z2}^{1.30}$
7	$^{6}Fe(acac)_3$	$d_{xy}^{1.14}d_{xz}^{1.16}d_{yz}^{1.16}d_{x2-y2}^{1.14}d_{z2}^{1.05}$

This suggests that a correct description of the Fe^{I} ion electronic structure cannot be obtained with a single electronic configuration, and is then beyond the limit of an accurate DFT analysis (see SI).[28] Nevertheless, several trends can be drawn from this analysis in the case of complexes **1a** and **1b**. The experimentally attested stability of the doublet state can indeed arise from the multiconfigurational character of the Fe^{I} center, counterbalancing the slight quartet stabilization predicted by DFT methods. Among the three examined candidates for (poly)phenyl arene-ligated Fe^{I} complexes (**1d**, **1e** and **1f**) which could account for the doublet species reported herein, a monophenyl species such as (η^6-C_6H_5Me)$Fe^{I}Ph$ seems unlikely since its structural topology is very close to Power's terphenyl complex (model **1d**), which has a strongly stabilized quartet ground state, as attested by EPR spectroscopy.[26a] Similarly to **1d**, DFT computation of (η^6-C_6H_6)$Fe^{I}Ph$ returns indeed a strong preference for the quartet configuration as well (18.7 kcal.mol^{-1} at the PBE0-D3/SDD level).[29,30] A triphenyl species [(η^6-arene)$Fe^{I}Ph_3$]$^{2-}$ (**1f**) seems also unlikely due to the strong stabilization of the quartet state (Scheme 8). However, in the case of the bis-phenyl analogue **1e**, the doublet-quartet gap is small enough (-1.1 to -9 kcal.mol^{-1} depending on the used functional) to consider multiconfigurational effects, similarly to **1a** and **1b**. Preliminary computational analysis run at CCSD(T) level indeed shows that the correlation energy is much stronger, by almost 0.1 a.u., in the doublet configuration of **1e** than in the quartet analogue. Such discrepancy between correlation effects involved in doublet and quartet electronic structures can lead to reinterpretation of the DFT-computed tendancies, mainly dominated by exchange energies and, therefore, favoring high-spin multiplicities. Small doublet-quartet DFT-computed gaps (complexes **1a**, **1b** and **1e**, Scheme 8) could therefore be counterbalanced by taking into account multiconfigurational effects. As highlighted by Bedford[4], monophenyl acac-ligated species such as [$PhFe^{I}$(acac)(THF)]$^{-}$ exhibits a strongly stabilized

quartet configuration with a computed doublet-quartet gap higher than 20 kcal.mol^{-1} (DFT level : PBE0 / 6-31+G(d) / SDD basis set and pseudopotential for Fe). This high gap could difficultly be overcome by multiconfigurational effects, and consequently, on the basis of the experimental and computational work reported herein, $[(\eta^6\text{-}C_6H_5Me)Fe^{I}Ph_2]^-$ seems to be a closer model for the description of the minor Fe^{I} species obtained upon reduction of a $Fe^{II/III}$ precursor with aryl Grignard reagents. Moreover, it is consistent with the recent report of Koszinowski et al. who reported that the $[Ph_2Fe^{I}]^-$ fragment could be detected by ESI mass spectroscopy when $Fe(acac)_3$ was reduced with PhMgCl in THF in cross-coupling conditions (presence of *i*PrCl as an electrophile).[19c] The determination of the structure of this Fe^{I} complex also allowed us to compute an estimation of the energetic barrier required to ensure the disproportionation of the tris-phenylated species $[Ph_3Fe^{II}]^-$ into the Fe^{III} and Fe^{I} oxidation states (thus affording $[Ph_4Fe^{III}]^-$ and $[(\eta^6\text{-}C_6H_5Me)Fe^{I}Ph_2]^-$) which was brought up by Koszinowski and Bedford (vide supra). At a DFT level (see SI), this reaction is quite athermic (ΔE = 0.2 kcal/mol), and could therefore occur in short times at room temperature.[31]

The plausibility of the bis-phenylated structure $[(\eta^6\text{-}C_6H_5Me)Fe^{I}Ph_2]^-$ depicted above (Scheme 7) has moreover been strengthened by the computation of its Mössbauer isomer shift following the DFT-based method mentioned in the previous section (ORCA 3.0.3 software, BP86 – TZVP / CP(PPP) for Fe atom). According to the calibration curve using the benchmark of Fe^0 and Fe^{I} complexes described earlier[25b], the computed density at the $^{57}Fe^{I}$ nucleus (ρ_0) for the structure $[(\eta^6\text{-}C_6H_5Me)Fe^{I}(Ph)_2]^-$ corresponds to a predicted isomer shift of 0.24 mm.s^{-1} (computed ρ_0: 11828.69 e.a_0^{-3}). This is in good agreement with the experimental value obtained from Mössbauer spectra (Figure 3) which was δ = 0.28 mm.s^{-1}.

Competition between η^6-toluene and η^6-biphenyl Fe^I ligations. As discussed earlier, the coordination of a η^6-biphenyl molecule onto the Fe^I ion cannot be ruled out in non-aromatic solvents such as THF. The competition between the coordination of toluene and biphenyl (i.e. the equilibrium between $[(\eta^6\text{-}C_6H_5Me)Fe^IPh_2]^-$ and $[(\eta^6\text{-}C_6H_5Ph)Fe^IPh_2]^-$) has been investigated by DFT (Scheme 9). The equilibrium is shifted towards the formation of the biphenyl species ^{PhPh}**1e**, with a slight stabilization of ca. 4.9 kcal.mol^{-1} with respect to the toluene analogue ^{Tol}**1e**. Therefore, it is likely that the coordination of the biphenyl molecule accumulated by oxidation of PhMgBr can occur in non-aromatic solvents, this ligand being replaced by a toluene molecule when the latter is used as a solvent.

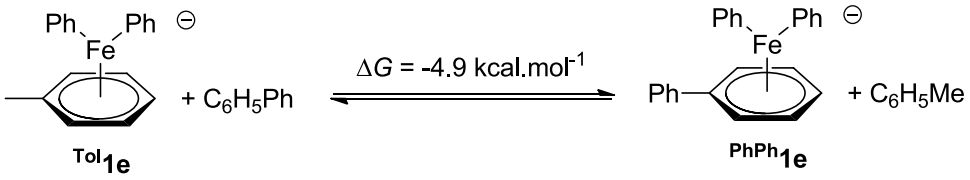

Scheme 9. Competition between the Fe^I-toluene and Fe^I-biphenyl ligation.

Very recently, the X-ray structure of the biphenyl complex ^{PhPh}**1e** was obtained by Hu et al. by reducing the iron-sulfur cluster $[Fe_4S_4Cl_4]^{2-}$ with an excess of phenyllithium. The authors moreover also assessed a low-spin ground state for this complex.[32]

Reactivity of *in-situ*-generated Fe^0 and Fe^I complexes in aryl-heteroaryl Kumada cross-couplings. The relevance of the complexes described in this article as possible active species in aryl-heteroaryl Kumada cross-couplings has been examined. 2-chloro-5-trifluoromethylpyridine (**HetArCl**) has been used as an electrophilic partner in catalytic conditions (Scheme 10):

chloropyridines proved indeed to be efficient cross-coupling partners in coligand-free iron-catalyzed methodologies.[2e]

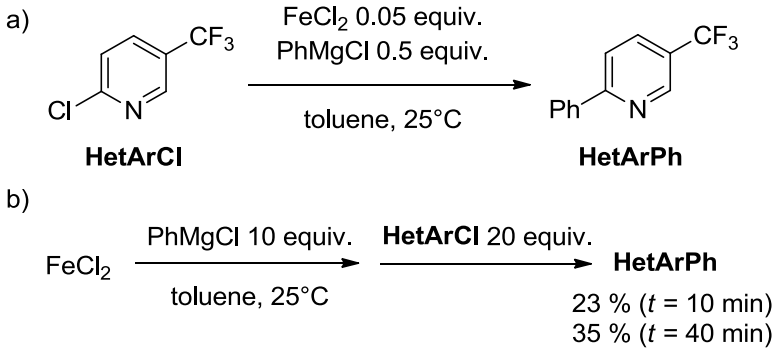

Scheme 10. Aryl-heteroaryl Kumada cross-coupling between PhMgCl and **HetArCl** investigated at room temperature (non-optimized conditions); a) catalytic one-pot conditions; b) step-by-step conditions with generation of Fe^0 prior to the addition of **HetArCl**. **HetArPh** yield calculated with respect to **HetArCl**.

In the one-pot catalytic conditions described above (Scheme 10a), a first Mössbauer spectrum with $^{57}FeCl_2$ as an iron source was recorded (Figure 7a).

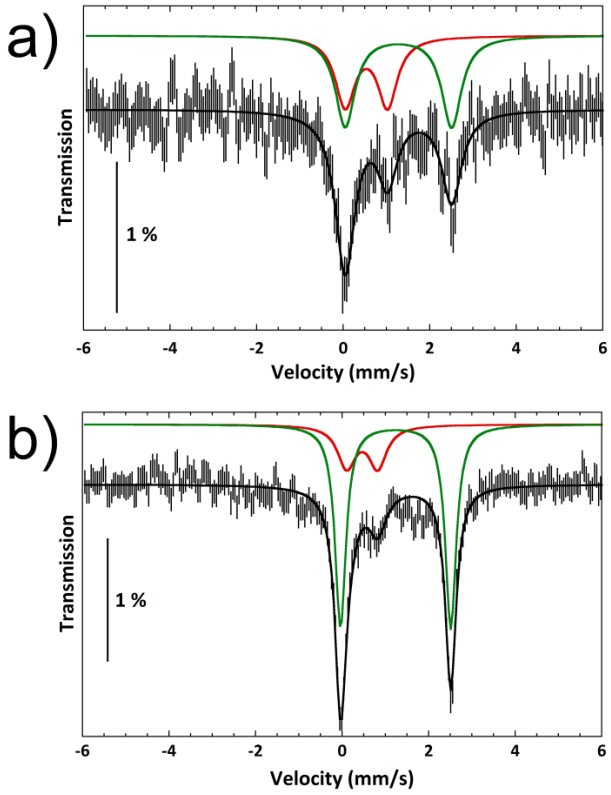

Figure 7. Mössbauer spectra at 80 K in toluene: a) solution containing $^{57}FeCl_2$ 2.5 mM and **HetArCl** (20 equiv.), frozen after addition of. PhMgCl (10 equiv., reaction time: 1 minute at rt); b) solution containing $^{57}FeCl_2$ reduced *in situ* by PhMgCl (10 equiv., reaction time: 3 minutes at rt) followed by addition of **HetArCl** (20 equiv.) and freezing (reaction time: 1 minute at rt). See the remarks regarding the low signal-to-noise ratio in the caption of Figure 3.

The spectrum displayed in Figure 7a exhibits a signal which could be simulated with two doublets. The first one (Figure 7a, red lines) accounts for ca. 39% of the overall iron quantity, with the following nuclear parameters: $\delta = 0.53$ mm.s^{-1}, $\Delta E_Q = 0.98$ mm.s^{-1}. This signal is well-fitted to the Fe^0 species described in the previous section, which featured similar parameters (Figure 3). The second doublet (Figure 7a, green lines) accounts for ca. 51% of the iron quantity with the following parameters: $\delta = 1.28$ mm.s^{-1}, $\Delta E_Q = 2.46$ mm.s^{-1}. This doublet corresponds to

the regenerated Fe^{II} precursor ($^{57}FeCl_2$) with nuclear parameters corresponding to a high-spin Fe^{II} center (see SI for the spectrum of $^{57}FeCl_2$). These data are gathered in the Table 5 (entry 1).

Table 5 . Best-fit parameters deduced from the simulation of the Mössbauer spectra displayed in Figures 7a (entry 1) and 7b (entry 2). An average error of ± 0.05 $mm.s^{-1}$ must be acknowledged in the simulations, due to the low signal-to-noise ratio of the experimental spectra.

Entry	Iron ox. state	Spin	δ ($mm.s^{-1}$)	ΔE_Q ($mm.s^{-1}$)	Γ ($mm.s^{-1}$)	% ± 5%
1	Fe^0	0	0.53	0.98	0.55	39
	Fe^{II}	2	1.28	2.46	0.55	51
2	Fe^0	0	0.46	0.75	0.50	24
	Fe^{II}	2	1.24	2.55	0.30	72

In agreement with the previous analysis, no transmetalated Ph—Fe^{II} species can be detected during catalysis (Figure 7a). However, at this point, the origin of the regeneration of the Fe^{II} precursor is unclear. Fe^{II} can indeed be provided by two drastically different pathways: it could either be formed by the reaction of the reduced Fe^0 species with the electrophile **HetArCl** (Scheme 11, path b) or come from the reaction of **HetArCl** with a transient, short-lived, phenylated organo-Fe^{II} intermediate formed prior to the Fe^0 oxidation state (Scheme 11, path a). In the second case, the bis-arene-ligated Fe^0 species would be an off-cycle intermediate.[33]

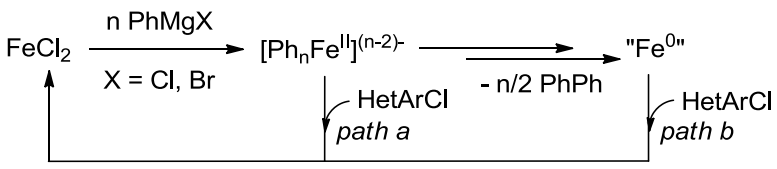

Scheme 11. Two possible pathways for the regeneration of $FeCl_2$ under catalytic conditions.

A second Mössbauer spectrum has therefore been recorded in order to examine selectively the reactivity of the Fe^0 species (Figure 7b), in the step-by-step conditions depicted in Scheme 10b. $^{57}FeCl_2$ has been reduced by an excess of PhMgCl to the Fe^0 oxidation state, and an excess of **HetArCl** has been added to the resulting solution, which was frozen after one minute at 25°C. It turned out that the same Fe^0 and Fe^{II} species are observed in both one-pot (Figure 7a) or step-by-step conditions (Figure 7b, see Table 5, entry 2). When Fe^0 is accumulated prior to the addition of the electrophile (conditions of Scheme 10b), the ratio Fe^{II} : Fe^0 slightly increases (3:1 *vs* 1.3:1 in the conditions of Scheme 10a). Therefore, the regeneration of the Fe^{II} precursor by reaction of the Fe^0 reduced species with the electrophile (Scheme 11, path b) seems to be operative at room temperature within a couple of minutes, and the formation of the cross-coupling product **HetArPh** was observed concomitantly (Scheme 10b).

cw-EPR spectra were also recorded in the conditions depicted in Scheme 10a, with non-enriched $FeCl_2$ as a precursor. These spectra showed that the Fe^I signal was not affected by the presence of 2-chloro-5-trifluoromethylpyridine. This result therefore suggests that the minor low-spin Fe^I species obtained in these coligand-free systems is actually an off-cycle species and does not contribute to catalytic processes involving aryl Grignard reagents and heteroaryl chlorides. In their recent report, Hu et al. demonstrated that the analogue biphenyl complex $[(\eta^6\text{-}C_6H_5Ph)Fe^IPh_2]^-$ was unreactive towards the addition of chloroarenes, but that stoichiometric C─C cross-coupling reactions could be observed while using organic bromides as electrophiles, albeit with low yield and concomitant formation of biphenyl.[32]

There is a strong similarity between the behavior of the SciOPP-stabilized systems reported by Neidig and the coligand-free systems investigated in this report. In both cases, the lowest oxidation state obtained upon reduction of Fe^{II} precursors by PhMgX (X = Cl, Br) is a Fe^{0} complex, which can be used as a precursor in Kumada-type catalytic cross-couplings. However, before stating that arene-ligated Fe^{0} complexes can be on-cycle intermediates in the case of coligand-free aryl-heteroaryl cross-coupling chemistry, the reactivity of transient, short-lived non-stabilized polyphenyliron(II) intermediates $[Ph_nFe^{II}]^{(n-2)-}$ must be investigated. It was indeed demonstrated that the SciOPP-stabilized analogues $(SciOPP)Fe^{II}(Ph)_n$ species were extremely reactive in Kumada and Suzuki-Miyaura cross-couplings[8] and that the reactivity of the zerovalent complex (η^6-biphenyl)Fe^{0}(SciOPP) was totally overwhelmed by the phenylated Fe^{II} complexes. Such investigations are currently in progress, and results will be reported in due time.

Concluding remarks

We established in this paper that several reduction mechanisms could take place when Fe^{II} or Fe^{III} salts were reduced by aryl Grignard reagents in the absence of a stabilizing co-ligand. In THF, $Fe(acac)_3$ undergoes a first ligand exchange with PhMgBr, leading to $PhFe(acac)_2$, which is prompt to lead to the formation of PhPh and $Fe(acac)_2$ in a dimeric pathway as suggested by DFT. The formation of PhPh involves a monoelectronic reduction of the Fe^{III} center, which can proceed by homolytic cleavage of $Ph-Fe^{III}$ bonds. A second phenyl transfer which would lead

from $PhFe(acac)_2$ to $[Ph_2Fe(acac)_2]^-$ requires an overall high energetic span which cannot be reached in the experimental conditions, making unlikely the possibility of a classic bielectronic reductive elimination directly connecting the Fe^{III} and Fe^{I} oxidation states. Fe^{I} can be obtained by further reduction of the Fe^{II} intermediates, as attested by cw-EPR spectroscopy in toluene:THF 10:1 mixtures. Unlike $Fe(acac)_3$, electron-deficient precursors $FeCl_2$ and $FeCl_3$ are more easily reduced by PhMgBr to the Fe^{I} level: $FeCl_3$ only requires 1 equiv. PhMgBr to provide Fe^{I} oxidation state, and $FeCl_2$ can also provide Fe^{I} by disproportionation of intermediate polyphenyliron(II) species. It was shown by EPR spectroscopy that the reduction of either $Fe(acac)_n$ or $FeCl_n$ (n = 2,3) led to a common low-spin Fe^{I} species regardless of the nature of the starting iron salt, suggesting a possible formation of a polyphenyliron(I) species. This complex has been proved to be unstable over time and represents moreover a minor fraction (ca. 15%) of the overall iron amount, as attested by EPR-based spin titration and Mössbauer spectroscopy. Mössbauer analysis actually shows that the distribution of the metallic species is quickly dominated after 3 minutes by diamagnetic iron(0) complexes. Computational analysis of the experimental Mössbauer data and compar ison with already reported mononuclear Fe^0 complexes allowed us to suggest that the major iron species detected herein featured Fe^0 centers which were stabilized by arene ligation, specifically by toluene when the latter was used as a solvent. The best model obtained by confronting experimental nuclear parameters and computed data was $(\eta^4\text{-}C_6H_5Me)_2Fe^0$. Due to the low signal-to-noise ratio of the Mössbauer spectra and the average error in the corresponding simulations, it can however be anticipated that multiple arene-stabilized Fe^0 species coexist in solution. The presence of several Fe^0 arene-ligated complexes was also confirmed by low-temperature ^1H NMR spectroscopy. These complexes are prompt to undergo aggregation, and finally provide iron nanoparticles. Structural data were also gained for

the minor Fe^{I} complex. Pulse EPR spectroscopy (HYSCORE) unambiguously demonstrates that the Fe^{I} ion is ligated by a toluene molecule, in a η^6-coordination. When iron salts were reduced with isotopically enriched $^{13}C_6H_5MgBr$, cw-EPR showed a significant broadening of the resonances due to hyperfine Fe^{I}—^{13}C coupling, attesting to a ligation of the Fe^{I} ion by σ-donating anionic $C_6H_5^-$ ligands. Analysis of the cw-EPR and HYSCORE hyperfine patterns suggests that the coordination sphere of the Fe^{I} ion involves two σ-ligated $C_6H_5^-$ ligands. This hypothesis was strengthened by DFT calculations and NBO analysis using different functionals (PBE0-D3, B3LYP-D3 and M06) as well as two pseudo-potentials for iron (SDD and CEP-31G). The evaluation of the quartet-doublet energetic gap was computed for a benchmark of low-spin and high-spin Fe^{I} complexes reported in the literature, showing that multiconfigurational effects were predominant for low-spin Fe^{I} species. On the basis of the experimental and computational results, a bis-phenyl structure $[(\eta^6\text{-}C_6H_5Me)Fe^{I}Ph_2]^-$ has been suggested. We moreover demonstrated that the $[(\eta^6\text{-}C_6H_5Me)Fe^{I}Ph_2]^-$ complex was not reactive in the aryl-heteroaryl Kumada cross-coupling conditions, since its concentration remained roughly constant upon addition of an heteroaryl chloride. On the other hand, the major bis-arene-ligated Fe^0 complex was able to react with 2-chloro-5-trifluoromethylpyridine and could be used as an efficient precursor for aryl-heteroaryl Kumada cross-couplings. The results reported in this paper are focused on the structural nature and the reactivity of the low-valent resting states which were observed at room temperature. The *in-situ* observation of transient short-lived intermediates at lower temperatures (such as polyphenyliron(II) species) and their relevance in similar catalytic processes are currently investigated.

ASSOCIATED CONTENT

Experimental procedures, parameters and softwares used for EPR and Mössbauer data analysis, as well as cartesian coordinates of optimized structures with the corresponding energies and lowest frequencies. This material is available free of charge via the Internet at http://pubs.acs.org.

AUTHOR INFORMATION

Corresponding Authors

* Guillaume Lefèvre, NIMBE, CEA, CNRS, Université Paris-Saclay, Gif-sur-Yvette, France

E-mail : guillaume.lefevre@cea.fr

* Pierre Dorlet, Institute for Integrative Biology of the Cell (I2BC), CEA, CNRS, Univ Paris-Sud, Université Paris-Saclay, Gif-sur-Yvette, France

E-mail : pierre.dorlet@cea.fr

* Jean-Marc Latour, University of Grenoble Alpes, LCBM/PMB and CEA, BIG/CBM/PMB and CNRS, LCBM UMR 5249, PMB, 38000 Grenoble, France

E-mail: jean-marc.latour@cea.fr

Author Contributions

The manuscript was written through contributions of all authors. All authors have given approval to the final version of the manuscript.

ACKNOWLEDGMENT

We acknowledge CEA, CNRS, the ANR (Project JCJC SIROCCO-16 (G.L.) and the French Infrastructure for Integrated Structural Biology (FRISBI; ANR-10-INSB-05-01) (P.D.)); Dr Pierre Thuéry (CEA) and Dr Christian Herrero (Univ. Paris-Sud Orsay) are thanked for technical assistance (X-Ray diffraction and EPR spectroscopy).

REFERENCES

(1) Bedford, R. B.; Brenner, P. B. *The development of iron catalysts for cross-coupling reactions*, in *Iron Catalysis II*, ed. Bauer, E., Springer Int, 2015.

(2) (a) Tamura, M.; Kochi, J. K. Vinylation of Grignard reagents. Catalysis by iron. *J. Am. Chem. Soc.* **1971**, *93*, 1487-1489; (b) Smith, R. S.; Kochi, J. K. Mechanistic studies of iron catalysis in the cross coupling of alkenyl halides and Grignard reagents. *J. Org. Chem.* **1976**, *41*, 502-509; (c) Quentin, J.; Franck, X.; Hocquemiller, R.; Figadère, B. Iron-catalysed arylation of heteroaryl halides by Grignard reagents. *Tet. Lett.* **2002**, *43*, 3547-3549; (d) Fürstner, A.; Leitner, A. Iron-Catalyzed Cross-Coupling Reactions of Alkyl-Grignard Reagents with Aryl Chlorides, Tosylates, and Triflates. *Angew. Chem. Int. Ed*. **2002**, *41*, 609-612; (e) Fürstner, A.; Leitner, A.; Mendez, M.; Krause, H. Iron-Catalyzed Cross-Coupling Reactions. *J. Am. Chem. Soc.* **2002**, *124*, 13856-13863; (f) Martin, R.; Fürstner, A. Cross-Coupling of Alkyl Halides with Aryl Grignard Reagents Catalyzed by a Low-Valent Iron Complex. *Angew. Chem. Int. Ed*. **2004**, *43*, 3955-3957; (g) Nakamura, M; Matsuo, K.; Ito, S.; Nakamura, E. Iron-Catalyzed Cross-Coupling of Primary and Secondary Alkyl Halides with Aryl Grignard Reagents. *J. Am. Chem. Soc.* **2004**, *126*, 3686-3687; (h) Nagano, T.; Hayashi, T. Iron-Catalyzed Grignard Cross-Coupling with Alkyl Halides Possessing β-Hydrogens. *Org. Lett*. **2004**, *6*, 1297-1299; (i) Sherry, B. D.; Fürstner, A. The Promise and Challenge of Iron-Catalyzed Cross Coupling. *Acc. Chem. Res*. **2008**, *41*, 1500-1511 (review); (j) Czaplik, W. M.; Mayer, M.; Cvengros, J.; von Wangelin, A. J. Coming of Age: Sustainable Iron-Catalyzed Cross-Coupling Reactions. *ChemSusChem* **2009**, *2*, 396-417 (review); (k) Kuzmina, O. M.; Steib, A. K.; Flubacher, D.; Knochel, P. Iron-Catalyzed Cross-Coupling of N-Heterocyclic Chlorides and Bromides with Arylmagnesium Reagents. *Org. Lett.* **2012**, *14*, 4818-4821; (l) Kuzmina, O. M.; Steib, A. K.; Markiewicz, J. T.; Flubacher, D.;

Knochel, P. Ligand-Accelerated Iron- and Cobalt-Catalyzed Cross-Coupling Reactions between N-Heteroaryl Halides and Aryl Magnesium Reagents. *Angew. Chem. Int. Ed.* **2013**, *52*, 4945-4949; (m) Nakamura, E.; Hatakeyama, T.; Ito, S.; Ishizuka, K.; Ilies, L.; Nakamura, M. *Org. React* **2014**, *83*, 1 (review); (n) Bauer, I.; Knölker, H.-J. Iron Catalysis in Organic Synthesis. *Chem. Rev.* **2015**, *115*, 3170-3387 (review).

(3) Hatakeyama, T.; Nakamura, M. Iron-Catalyzed Selective Biaryl Coupling: Remarkable Suppression of Homocoupling by the Fluoride Anion. *J. Am. Chem. Soc*. **2007**, *129*, 9844-9845.

(4) Bedford, R. B. How Low Does Iron Go? Chasing the Active Species in Fe-Catalyzed Cross-Coupling Reactions. *Acc. Chem. Res.* **2015**, *48*, 1485-1493.

(5) Fürstner, A.; Krause, H.; Lehmann, C. W. Unusual Structure and Reactivity of a Homoleptic "Super-Ate" Complex of Iron: Implications for Grignard Additions, Cross-Coupling Reactions, and the Kharasch Deconjugation. *Angew. Chem. Int. Ed.* **2006**, *45*, 440-444.

(6) (a) Adams, C. J.; Bedford, R. B.; Carter, E.; Gower, N. J.; Haddow, M. F.; Harvey, J. N.; Huwe, M.; Cartes, M. A.; Mendoza, C.; Murphy, D. M.; Neeve, E. C.; Nunn, J. Iron(I) in Negishi Cross-Coupling Reactions. *J. Am. Chem. Soc.* **2012**, *134*, 10333-10336; (b) Bedford, R. B.; Carter, E.; Cogswell, P. M.; Gower, N. J.; Haddow, M. F.; Harvey, J. N.; Murphy, D. M.; Neeve, E. C.; Nunn, J. Simplifying Iron–Phosphine Catalysts for Cross-Coupling Reactions. *Angew. Chem. Int. Ed.* **2013**, *52*, 1285-1288.

(7) (a) Kleimark, J.; Hedström, A.; Larsson, P.-F.; Johansson, C.; Norrby, P.-O. Mechanistic Investigation of Iron-Catalyzed Coupling Reactions. *ChemCatChem* **2009**, *1*, 152-161; (b) Guisán-Ceinos, M.; Tato, F.; Buñuel, E.; Calle, P.; Càrdenas, D. J. Fe-catalysed Kumada-type alkyl–alkyl cross-coupling. Evidence for the intermediacy of Fe(I) complexes. *Chem. Sci.* **2013**, *4*, 1098-1104; (c) Hedström, A.; Izakian, Z.; Vreto, I.; Wallentin, C.-J.; Norrby, P.-O.

On the Radical Nature of Iron-Catalyzed Cross-Coupling Reactions. *Chem. Eur. J.* **2015**, *21*, 5946-5953; (d) Noda, D.; Sunada, Y.; Hatakeyama, T.; Nakamura, M.; Nagashima, H. Effect of TMEDA on Iron-Catalyzed Coupling Reactions of ArMgX with Alkyl Halides. *J. Am. Chem. Soc.* **2009**, *131*, 6078-6079; (e) Liu, Y.; Xiao, J.; Wang, L.; Song, Y.; Deng, L. Carbon−Carbon Bond Formation Reactivity of a Four-Coordinate NHC-Supported Iron(II) Phenyl Compound. *Organometallics* **2015**, *34*, 599-605; (f) Liu, Y.; Wang, L.; Deng, L. Three-Coordinate Iron(II) Dialkenyl Compound with NHC Ligation: Synthesis, Structure, and Reactivity. *Organometallics* **2015**, *34*, 4401-4407; (g) Liu, Y.; Luo, L.; Xiao, J.; Wang, L.; Song, Y.; Qu, J.; Luo, Y.; Deng, L. Four-Coordinate Iron(II) Diaryl Compounds with Monodentate *N*-Heterocyclic Carbene Ligation: Synthesis, Characterization, and Their Tetrahedral-Square Planar Isomerization in Solution. *Inorg. Chem.* **2015**, *54*, 4752-4760.

(8) Daifuku, S. L.; Kneebone, J. L.; Snyder, B. E. R.; Neidig, M. L. Iron(II) Active Species in Iron–Bisphosphine Catalyzed Kumada and Suzuki–Miyaura Cross-Couplings of Phenyl Nucleophiles and Secondary Alkyl Halides. *J. Am. Chem. Soc.* **2015**, *137*, 11432-11444.

(9) Muñoz III, S. B.; Daifuku, S. L.; Brennessel, W. W.; Neidig, M. L. Isolation, Characterization, and Reactivity of $Fe_8Me_{12}^-$: Kochi's S = 1/2 Species in Iron-Catalyzed Cross-Couplings with MeMgBr and Ferric Salts. *J. Am. Chem. Soc.* **2016**, *138*, 7492-7495.

(10) SimuMoss software. Charavay, C.; Segard, S.; Edon, F.; Clémancey, M.; Blondin, G. CEA/DRF/BIG, CNRS, Univ. Grenoble Alpes.

(11) Williamson, K. L.; Masters, K. M. *Macroscale and microscale organic experiments, 6th edition*, Cengage Learning, 2010.

(12) Xue, Z.; Daran, J.-C.; Champouret, Y.; Poli, R. Ligand Adducts of Bis(acetylacetonato)iron(II): A ^{1}H NMR Study. *Inorg. Chem.* **2011**, *50*, 11543-11551.

(13) It was reported by Neidig that an *in-situ* acidic quenching at short times (within ca. 30 s, see ref. (8)) could artificially lead to the formation of biphenyl, thus leading to an overestimation of its quantity formed by reduction of iron. This is due to the quenching process of transient short-lived aryliron(II) species.

(14) (a) Carloni, P.; Greci, L.; Stipa, P.; Electron-Transfer Reactions. Oxidation of Grignard Reagents in the Presence of an Aminoxyl as a Radical-Trapping Agent. *J. Org. Chem.* **1991**, *56,* 4733-4737, and references cited; (b) Lefèvre, G.; Jutand, A. Activation of Aryl and Heteroaryl Halides by an Iron(I) Complex Generated in the Reduction of [$Fe(acac)_3$] by PhMgBr: Electron Transfer versus Oxidative Addition. *Chem. Eur. J.* **2014**, *16,* 4796-4805; (c) This is confirmed by a DFT-computed barrier of 45.1 $kcal.mol^{-1}$. Grignard reagents can act as monoelectronic reductants with oxidants weaker than $Fe(acac)_3$, but under harsher conditions. See: Eberson, L. Experimental Evidence for an Electron-Transfer Mechanism in the Reaction between 2-Phenyl-3-(phenylimino)-3H-indole and Grignard Reagents: Application of the Marcus Theory. *J. Org. Chem.* **1984**, *49,* 2135-2139 (oxidation of alkyl Grignard reagents by iminoindoles); Uchiyama, N.; Shirakawa, E.; Hayashi, T. Single electron transfer-induced Grignard cross-coupling involving ion radicals as exclusive intermediates. *Chem. Comm.* **2013**, *49,* 364-366 (oxidation of PhMgBr by aryl iodides); see also ref. (14a) for oxidation of Grignard reagents by indole bisnitrone; (d) A bis-aryl magnesium species such as Ph_2Mg, *in-situ*-formed by Schlenk equilibrium, could more likely be involved in outer-sphere monoelectronic transfers with $Fe(acac)_3$. Bis-organomagnesium compounds are indeed more easily oxidized than their Grignard analogues, see Psarras, T.; Dessy, R. E. Organometallic Electrochemistry. X. Organomagnesium reagents. *J. Am. Chem. Soc.* **1966**, *88*, 5132-5135.

(15) *Transition Metal Arene π-Complexes in Organic Synthesis and Catan lysis,* ed. Kündig,

E. P., Springer Int, 2004.

(16) (a) for the formation of a well-defined tetraaryliron(III) species, see Alonso, P. J.; Arauzo, A. B.; Fornies, J.; Garcia-Monforte, M. A.; Martin, A.; Martinez, J. I.; Menjon, B.; Rillo, C.; Saiz-Garitaonandia, J. J. A Square-Planar Organoiron(III) Compound with a Spin-Admixed State. *Angew. Chem., Int. Ed*. **2006**, *45*, 6707-6711; (b) For the formation of $[Me_4Fe^{III}]^-$ anion by transmetallation of MeMgBr onto $FeCl_3$, see Al-Afyouni, M. H.; Fillman, K. L.; Brennessel, W. W.; Neidig, M. L. Isolation and Characterization of a Tetramethyliron(III) Ferrate: An Intermediate in the Reduction Pathway of Ferric Salts with MeMgBr. *J. Am. Chem. Soc.* **2014**, *136*, 15457-15460.

(17) (a) Smith, J. M.; Sadique, A. R.; Cundari, T. R.; Rodgers, K. R.; Lukat-Rodgers, G.; Lachicotte, R. J.; Flaschenriem, C. J.; Vela, J.; Holland, P. L. Studies of Low-Coordinate Iron Dinitrogen Complexes. *J. Am. Chem. Soc*. **2006**, *128*, 756-769; (b) Lichtenberg, C.; Viciu, M.; Adelhardt, L.; Sutter, J.; Meyer, K.; de Bruin, B.; Grützmacher, H. Low-Valent Iron(I) Amido Olefin Complexes as Promotors for Dehydrogenation Reactions. *Angew. Chem. Int. Ed.* **2015**, *54*, 5766-5771.

(18) The structure was isomorph of the chloride analogue reported in Döring, M.; Uhlig, E.; Dahlenburg, L. Die binuklearen Produkte der Umsetzung von Grignardreagenzien mit Acetylacetonaten der späten 3d-Elemente und ihre katalytische Wirkung bei der Kreuzkopplung. *Z. Anorg. Allg. Chem.* **1989**, *578*, 58-68.

(19) (a) for the formation of polyphenyl-Fe^{II} species using PhLi, see Fürstner, A.; Martin, R.; Krause, H.; Seidel, G.; Goddard, R.; Kehmann, C. W. Preparation, Structure, and Reactivity of Nonstabilized Organoiron Compounds. Implications for Iron-Catalyzed Cross Coupling Reactions. *J. Am. Chem. Soc.* **2008**, *130*, 8773-8787; (b) Bedford, R. B.; Brenner, P. B.; Carter,

E.; Cogswell, P. M.; Haddow, M. F.; Harvey, J. N.; Murphy, D. M.; Nunn, J.; Woodall, C. H. TMEDA in Iron-Catalyzed Kumada Coupling: Amine Adduct versus Homoleptic "ate" Complex Formation. *Angew. Chem. Int. Ed*. **2014**, *53*, 1804-1808; (c) Parchomyk, T.; Koszinowski, K. Ate Complexes in Iron-Catalyzed Cross-Coupling Reactions. *Chem. Eur. J.* **2016**, *22*, 15609-15613.

(20) (a) Schilter, D.; Nilges, M. J.; Chakrabarti, M.; Lindahl, P. A.; Rauchfuss, T. B.; Stein, M. Mixed-Valence Nickel−Iron Dithiolate Models of the [NiFe]-Hydrogenase Active Site. *Inorg. Chem.* **2012**, *51*, 2338-2348; (b) Silakov, A.; Olsen, M. T.; Sproules, S.; Reijerse, E. J.; Rauchfuss, T. B.; Lubitz, W. EPR/ENDOR, Mössbauer, and Quantum-Chemical Investigations of Diiron Complexes Mimicking the Active Oxidized State of [FeFe]Hydrogenase. *Inorg. Chem.* **2012**, *51*, 8617-8628 ; (c) Stoian, S. A.; Hsieh, C.-H.; Singleton, M. L.; Casuras, A. F.; Darensbourg, M. Y.; McNeely, K.; Sweely, K.; Popescu, C. V. Hyperfine interactions and electron distribution in $Fe^{II}Fe^{I}$ and $Fe^{I}Fe^{I}$ models for the active site of the [FeFe] hydrogenases: Mössbauer spectroscopy studies of low-spin Fe^{I}. *J Biol Inorg Chem* **2013**, *18*, 609–622.

(21) (a) Bedford, R. B.; Brenner, P. B.; Carter, E.; Clifton, J.; Cogswell, P. M.; Gower, N. J.; Haddow, M. F.; Harvey, J. N.; Kehl, J. A.; Murphy, D. M.; Neeve, E. C.; Neidig, M. L.; Nunn, J.; Snyder, B. E. N.; Taylor, J. Iron Phosphine Catalyzed Cross-Coupling of Tetraorganoborates and related Group 13 Nucleophiles with Alkyl Halides. *Organometallics* **2014**, *33*, 5767-5780; (b) Ouyang, Z.; Meng, Y.; Cheng, J.; Xiao, J.; Gao, S.; Deng, L. Three- and Four-Coordinate Homoleptic Iron(I)–NHC Complexes: Synthesis and Characterization. *Organometallics* **2016**, *35*, 1361-1367.

(22) (a) Parker, S. F.; Peden, C. H. F. Iron benzene reactions: a matrix isolation Mössbauer investigation. *J. Organomet. Chem.* **1984**, *212*, 411-416; (b) Blom, B.; Tan, G.; Enthaler, S.; Inoue, S.; Epping, J. D.; Driess, M. Bis‐N‐Heterocyclic Carbene (NHC) Stabilized η^6‐Arene

Iron(0) Complexes: Synthesis, Structure, Reactivity, and Catalytic Activity. *J. Am. Chem. Soc*. **2013**, *135*, 18108−18120.

(23) Michaud, P.; Mariot, J.-P.; Varret, F.; Astruc, D. Improved Synthesis and Electronic Structure of the 19- and 20-Electron Complexes $[Fe(\eta^6\text{-}C_6Me_6)_2]^{n+}$, n = 0,1. *J. Chem. Soc., Chem. Commun.* **1982**, 1383-1385.

(24) (a) Ittel, S. D.; Tolman, C. A. Metal Vapor Synthesis of Iron η^6-Arene Complexes. *Organometallics* **1982**, *1*, 1432-1436; (b) Morand, P. D.; Francis, C. G. Modeling Macroscale Metal Vapor Reactions. 2. Bis(arene)iron Revisited. *Organometallics* **1985**, *4*, 1653-1659.

(25) (a) Römelt, M.; Ye, S.; Neese, F. Calibration of Modern Density Functional Theory Methods for the Prediction of ^{57}Fe Moössbauer Isomer Shifts: Meta-GGA and Double-Hybrid Functionals. *Inorg. Chem*. **2009**, *48*, 784-785, and references cited; (b) low-spin Fe^0 complexes: $Fe(CO)_5$, $(\eta^4\text{-}C_4H_4)Fe(CO)_3$, $(\eta^6\text{-}C_6H_6)(\eta^4\text{-}C_6H_8)Fe$, $(\eta^6\text{-}C_6H_6)(\eta^4\text{-}C_6H_6)Fe$, ($\eta^6$-biphenyl)Fe(SciOPP), Fe(bis-(N-(2,6-diisopropylphenyl)-imidazole-2-ylidene)methylene)(η^6-C_6H_6); high-spin Fe^0 complex: $(\eta^6\text{-}C_6Me_6)_2Fe$; low-spin Fe^I complexes: (p-tolyl)$(Ph_2PCH_2CH_2PPh_2)_2Fe$, $NaFe(trop_2dae)(THF)_3$ (trop=5*H*-dibenzo[*a*,*d*]cyclo-hepten-5-yl, dae=(N-CH_2-CH_2-N)); see SI for the corresponding reported nuclear parameters and the related references; (c) Computation of the quadrupolar split was more problematic since this nuclear parameter is highly dependant on the symmetry of the occupied electronic levels. For several complexes in the benchmark depicted earlier (ref. (25b)), the experimental value of ΔE_Q could not be reproduced with a satisfying accuracy. Therefore, minor differences between the optimized geometries and the experimental structures can induce strong discrepancies between the experimental and calculated values of ΔE_Q. For a report of computational analysis of quadrupolar splits, see : Pàpai, M.; Vankò, G. On Predicting Mössbauer Parameters of Iron-

Containing Molecules with Density-Functional Theory. *J. Chem. Theor. Comp.* **2013**, *9*, 5004-5020.

(26) (a) Ni, C.; Ellis, B. D.; Fettinger, J. C.; Long, G. J.; Power, P. P. Univalent transition metal complexes of arenes stabilized by a bulky terphenyl ligand: differences in the stability of Cr(I), Mn(I) or Fe(I) complexes. *Chem. Commun.* **2008**, 1014-1016; (b) Gunnar Werncke, C.; Bunting, P. C.; Duhayon, C.; Long, J. R.; Bontemps, S.; Sabo-Etienne, S. Two-Coordinate Iron(I) Complex $[Fe\{N(SiMe_3)_2\}_2]^-$: Synthesis, Properties, and Redox Activity. *Angew. Chem. Int. Ed.* **2015**, *54*, 245-248.

(27) (a) **1a** is a model for $(\eta^6\text{-}C_6H_6)Fe^I(HC(C[Me]N\text{-}(2,6\text{-diisopropylphenyl}))_2)$ and **1c** for its PPh_3-analogue; see ref. (17a); (b) for **1b**: see ref. (17b); c) **1d** is a model for $(\eta^6\text{-}C_6H_6)Fe^I(C_6H\text{-}2,6\text{-}(C_6H_2\text{-}2,4,6\text{-}iPr_3)_2\text{-}3,5\text{-}iPr_2)$), see ref. (26a).

(28) Schmidt, M. W.; Gordon, M. S. The construction and interpretation of MCSCF wavefunctions. *Annu. Rev. Phys. Chem.* **1998**, *49*, 233-266.

(29) The same conclusion was reported by Norrby regarding $PhFe^I(THF)_n$ complexes: Hedström, A.; Lindstedt, E.; Norrby, P.-O. On the oxidation state of iron in iron-mediated C–C couplings. *J. Organomet. Chem.* **2013**, *748*, 51-55.

(30) Moreover, computed density at the ^{57}Fe nucleus in monophenyl spin doublet species $(\eta^6\text{-}C_6H_6)Fe^IPh$ would lead to an isomer shift of 0.67 $mm.s^{-1}$ (computed ρ_0 : 11827.64 $e.a_0^{-3}$) which is strongly different of the experimental value.

(31) $[Ph_3Fe^{II}]^-$ has been computed in the quintet spin state, which is the usual spin state for tris-hydrocarbyl ate-Fe^{II} species, see ref. 19b and references cited therein. A sextet ground state has been found for $[Ph_4Fe^{III}]^-$; $[(\eta^6\text{-}C_6H_5Me)Fe^IPh_2]^-$ has been computed in the doublet state.

(32) Zhurkin, F. E.; Wodrich, M. D.; Hu, X. A Monometallic Iron(I) Organoferrate.

Organometallics **2017**, *36*, 499-501.

(33) This second scenario is preferred for the aryl-alkyl Kumada coupling mediated by SciOPP-Fe^{II} systems, see ref 8.

FOR TABLE OF CONTENTS ONLY

The formation of arene-stabilized iron(0) and iron(I) complexes obtained by reduction of iron salts with aryl Grignard reagents in the absence of stabilizing co-ligand is reported. Their structures are investigated by cw-EPR, HYSCORE, ^{1}H NMR and Mössbauer spectroscopies and by DFT computations. The presence of an arene ligation by solvent molecules is demonstrated for the first time in such systems. The reactivity of these complexes in catalytic aryl-heteroaryl Kumada coupling is investigated.